UNIVERSITY OF CRETE
DEPARTMENT OF PHYSICS

FOUNDATION FOR RESEARCH AND TECHNOLOGY HELLAS
INSTITUTE OF ELECTRONIC STRUCTURE AND LASER

BACHELOR THESIS

«Fabrication of 3D structures of ZnO nanorods for gas sensing at room temperature»

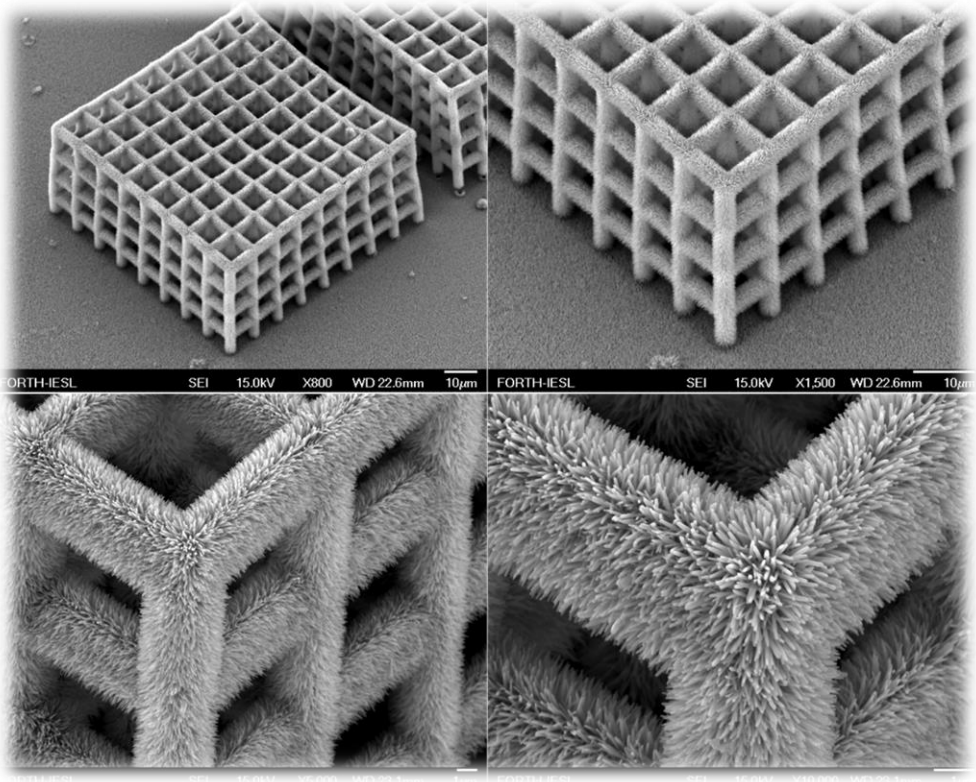

IOANNIS SYNGELAKIS

Supervisors: Argiro Klini, Maria Farsari

HERAKLION OCTOBER 2019

ΕΥΧΑΡΙΣΤΙΕΣ

Η πραγματοποίηση της πτυχιακής διπλωματικής μου εργασίας έγινε εφικτή με την καθοδήγηση και την βοήθεια κάποιων ανθρώπων, χωρίς την συμπαράσταση των οποίων δεν θα ολοκληρωνόταν αυτή η προσπάθεια και θα ήθελα να τους ευχαριστήσω. Την Δρ. Μαρία Φαρσάρη, ερευνητικός διευθυντής και αρχηγός της ομάδας «Μη-γραμμικής Λιθογραφίας» στο Ινστιτούτο Ηλεκτρονικής Δομής και Laser - FORTH, για την δυνατότητα που μου έδωσε να μάθω πράγματα και να εκπαιδευτώ στο εργαστήριο της καθώς για την καθοδήγηση στα περισσότερα βήματα της εργασίας μου. Την Δρ. Αργυρώ Κλίνη, κύριος ερευνητής στο Ινστιτούτο Ηλεκτρονικής Δομής και Laser - FORTH, για την υπομονή, την συνεργασία και την υποστήριξη της, καθ' όλη την διάρκεια της εργασίας. Την υπόλοιπη ομάδα της «Μη-γραμμικής Λιθογραφίας», για την προθυμία τους να βοηθήσουν το πρώτο διάστημα της εκπαίδευσης μου στο εργαστήριο, αλλά και στην άριστη συνεργασία και το ευνοικό περιβάλλον που υπήρχε μεταξύ μας κατά την διάρκεια της. Τον Δρ. Γεώργιο Κενανάκη, κύριος ερευνητής στο Ινστιτούτο Ηλεκτρονικής Δομής και Laser – FORTH, για την επιστημονική του βοήθεια και τις συμβουλές του για την ανάπτυξη των νανοράβδων από ZnO. Επίσης, θα ήθελα να εκφράσω ένα θερμό ευχαριστώ στην κα. Αλέκα Μανουσάκη, για την συμπαράσταση,υποστήριξη και την συνεργασία κατά τις ατελείωτες ώρες των μετρήσεων στο ηλεκτρονικό μικροσκόπιο σάρωσης (SEM) και για τις μετρήσεις στο προφιλόμετρο. Τέλος, την Δρ. Μαρία Ανδρουλιδάκη για την παροχή βοήθειας και την λήψη μετρήσεων Photoluminescence των 3D δομών επικαλυμένων με νανοράβδους από ZnO.

Abstract

The purpose of this work is fabrication of 3D structures consist of Zinc Oxide (ZnO) nanorods. These devices would be employed for gas sensing at room temperature due to the potential increase in active surface area. There were results from research which have revealed that surfaces, covered by ZnO semiconductor, present sensing behavior. Also, there have been work in construction of 3D arrays of ZnO nanorods in the past but only its photocatalytic performance was investigated. That is why 3D scaffolds were fabricated in order to serving us substrates for growth of ZnO nanorods and examine the sensing behavior of ZnO on complex geometries. The aim is to increase of sensing behavior this semiconductor exhibits by increasing the surface area through which the semiconductor interacts with the environment.

For the accomplishment of this work three main methods have been adopted. Firstly, the 3D scaffolds were constructed using Multiphoton Lithography (MPL) technique and the next step was deposition of seed Zn layer utilizing Pulsed Laser Deposition (PLD) technique. Finally, hydrothermal growth of ZnO nanorods was achieved by Aqueous Chemical Growth (ACG) technique. MPL is a direct laser writing technique for fabrication of 3D scaffolds with features on submicron scale with great accuracy. The idea is that phase transition from gel state to solid state can be occurred via multiphoton polymerization of photosensitive materials. After a special treatment, only the light exposed material can be remained with the final result the desire 3D structures. PLD is a physical vapor deposition procedure for thin films growth. It is a light-induced process in which stoichiometric transfer is achieved through vaporization of a material. Only requirements are a bulk target material, a substrate, a pulsed laser source and vacuum conditions and a pure layer of desired material can be deposited into a substrate. The role of seed Zn layer from PLD is crucial for uniformly growth of nanorods on substrates. ACG is a solution growth technique, which is a quite simple method for growth of nanostructures. It is taken place at relatively low temperatures, presenting several advantages such as the use of non-expensive equipment, the requirement of cheap and non-toxic reagents and the presence of non-hazardous by-products.

Contents

Chapter 1
Multiphoton Lithography

1.1 Introduction

Stereolithography historically refers to the technology where three-dimensions (3D) objects converted from designs into real products via computed aided design (CAD)[1,2]. In conventional stereolithography[3], photopolymerization is induced by interaction between a ultraviolet (UV) laser beam and a photosensitive material result in a phase transition process. When an appropriate material (resin which consists of monomer units) in liquid or gel-state is photocured at a spot, converted into a solid-state polymer. By scanning the laser beam three-dimensionally through the material, inducing selectively photopolymerization, 3D structures can be fabricated. Also, there are disadvantages for the use of this method as the increasing technology advantages require devices in the smallest possible scale with complex features. Classical stereolithography and other 3D prototyping techniques such as: 3D inject printing[4,5] or e-beam lithography[6,7] can also produce 3D structures but with poor resolution or complication respectively. In contrast, via multiphoton photon fabrication method (MPF)[8,9], fabrication resolution can be accomplished beyond diffraction limit of light. This could have many applications in research nowadays. Photonic crystals[10–13],sensor devices[14–18], metamaterials[19], scaffolds for biological research[20–22] and tissue engineering[21,23] or photocatalytic applications[14] and microfluidics[24] can be constructed with this method.

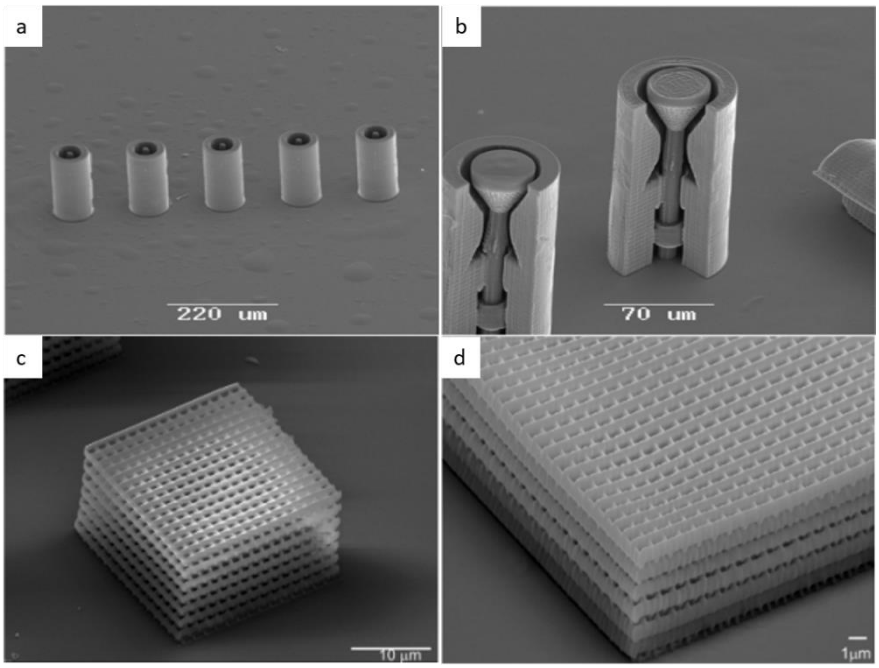

Figure 1.1: Sem images of 3D structures fabricated by MPP in microscale. Images a),b) show valves could be used in microfluidics research. Images c),d) show a photonic crystal which can be served as micromechanical device.

In this work as referred above, MPF method is employed in order to fabricate 3D structures which were used as substrates. This is a direct laser writing technique which is based on multiphoton polymerization (MPP) of a photosensitive material. Its special feature is that fabrication accuracy can be lower than 100nm combining a great complexity in fabrication geometry. MPP is the result of another process, which is called multiphoton absorption (MPA). During MPA, there is non-linear absorption of light irradiation by material, so two or more photons can impact enough energy for an electron transition. Through these excitations a polymerization process could be initiated with result a phase transition of the material. Via polymerization, a material in liquid or gel-state could be converted into solid-state. The difference of the other lithographic methods is that polymerization is induced from nonlinear interactions between light from a laser beam and materials used.

There is analogy between MPA of n photons and the rate of a concerted chemical reaction involving n molecules, generally the n-photon absorption leads to n-photon polymerization[25]. As a result, the rate of MPA for n photons is proportional to light intensity (number of photons per volume per time) to nth power[26]. In order to accomplish these nonlinear phenomena, high light intensities are required due to the very small cross-section of the process. Thus, the use of a laser beam as an excitation source is essential. When a laser beam is tightly focused onto a volume of photopolymerizable material, the polymerization process can be initiated by nonlinear absorption of light irradiation. Only if the energy of all absorbed photons is equal or transcend the energy difference of energy levels between the ground state and the first excited state, an electron excitation can occur. That is why MPF also called Non-Linear Lithography (NLL), which in contrast to the others lithographic techniques benefits from non-linear phenomena to achieve 3D patterning with spatial control.

An example of MPP processes is the two-photon polymerization[27,28] (TPP). TPP is carried out by two-photon absorption (TPA) when a beam from ultrafast laser is tightly focused onto a transparent, photosensitive resin. The TPA rate is proportional to the square of the light intensity so TPA can take place only inside the focal volume. The TPP occurs when the laser intensity is high enough so the polymerization threshold of the material satisfied. Therefore, due to highly localization of reaction volume (voxel), features with high resolution can be obtained. The transparency of the material to the laser spectral region is necessary for the technique because with the move of the focal volume three-dimensionally through the sample, 3D structures can be prepared without effecting the rest of the sample. Two different experimental set ups were utilized for the process and both of them were controlled by a computer software where the desired pattern can be defined. After the selected expose under light radiation and material polymerization, the unpolymerized resin is needed to remove and this is accomplished by immersing the sample into an appropriate solvent so the 3D structures have been remained.

1.2 Two-photon absorption

As referred above, when the excitation energy comes from one-photon absorption (OPA), one-photon polymerization (OPP) result in. In this case, the incident light irradiation is absorbed by the material[29] following the Beer-Lambert law. As a result, OPP is a material processing method that can only take place on the surface of a sample, that is why implementation of OPP can't give the ability to in-volume patterning and creating complicate 3D structures.

By the same token the excitation can be accomplished by absorbing two photons at longer wavelength in order to offer the same energy. Usually the energy difference between the ground and the first excited state for a common resin corresponds to a UV photon. This energy could also be equal to the sum of the energies of two near red-infrared (NIR) photons. In case of TPA, two-photon polymerization (TPP) could be induced via light irradiation from a laser beam in the red-infrared spectral region as an excitation source.

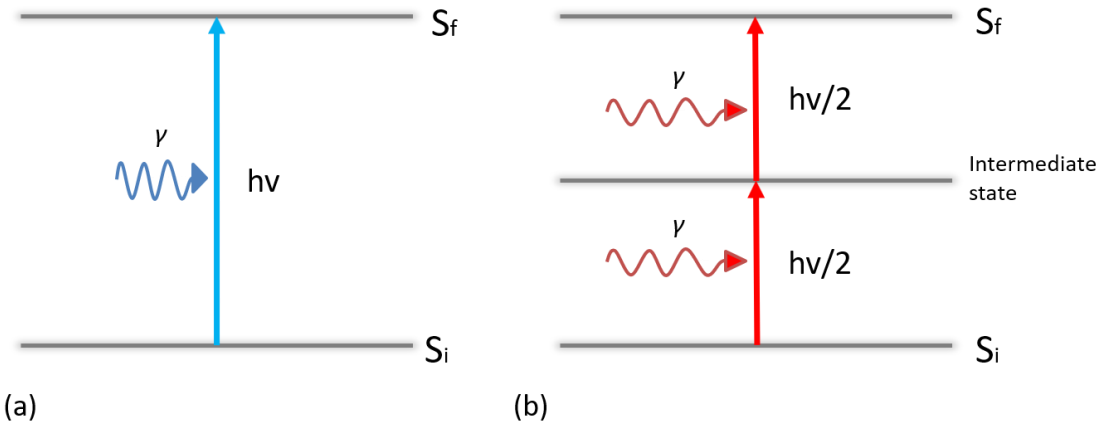

Figure 1.2: Illustration of one-photon absorption (a) and two-photon absorption (b). TPA occurs via an intermediate state between the absorptions of first and second photon. In this case, the electron transition is caused by two photons of energy hv/2, rather than one of energy hv and as result the two photons wavelengths are 2λ where λ is the excitation wavelength in OPA.

According to the nature of intermediate state, the electron excitations via TPA can be accomplished with two ways. If this state is real the TPA process called sequential, otherwise called simultaneous. The existence of a real intermediate state implies that the material, which is used in the fabrication process, absorbs in that spectral region, so the case of sequential TPA should have similar characteristics and results to OPA.

In simultaneous TPA, a virtual state is formed when the first photon is absorbed and the excitation to the final state happens only if the time distance until second photon's arrival isn't longer than the lifetime of virtual state. The lifetime's order of magnitude can be predicted from the Heisenberg's uncertainty principle. Considering that the state's energy level should be around 10^{-1} eV, its estimated lifetime is of the order of few femtoseconds[1]. Due to virtual state's short lifetime the cross-section of a simultaneous TPA is small. Thus, high light intensities (high photon densities per time) are required to increase the possibility simultaneous TPA happens.

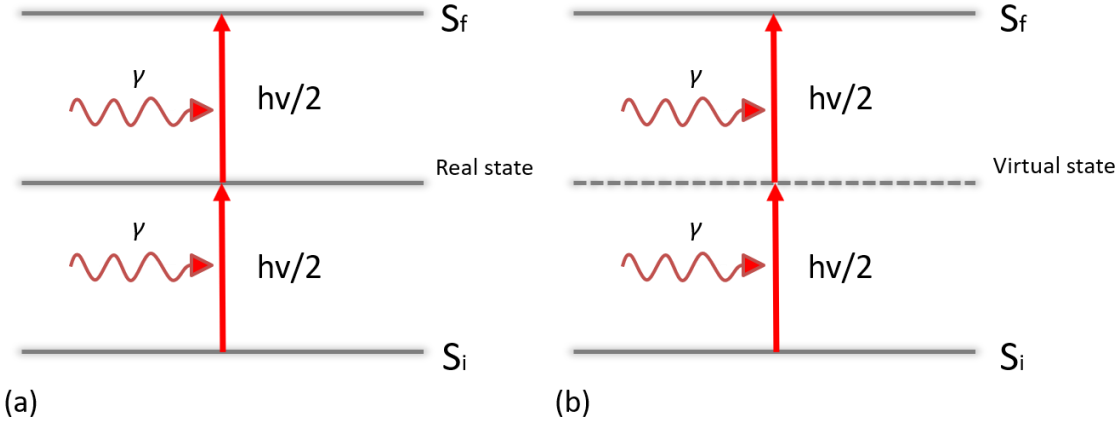

Figure 1.3: Sequential TPA (a) and simultaneous TPA (b). In the latter case the intermediate state is virtual unlike the first one. It's essential for this to happen, a laser beam with short pulse duration closely focused onto a volume of transparent, photosensitive material.

High light intensities can only be provided from a tightly focused laser beam with short pulse duration. Thereby, ultrafast lasers usually employed to drive MPA processes. A typical femtosecond laser with pulses of the order of several femtoseconds (fs), can provide instantaneous light intensity which is favorable for MPA processes. Irradiation from a femtosecond laser can provide fast absorption of the incident photon energy except of high photon densities per time. Typical time needed that the excited electrons can transfer energy to the lattice of absorbing species through phonon emission is few picoseconds (ps). Irradiation by femtosecond pulses meaning that the excitation is a heat insulation process. Although, lasers with longer pulse duration can be used, they produce thermal effects which are processes difficult to localize so are not desired.

Generally, the rate of nth-photon absorption in a transverse cross-section of a laser beam depends upon the nth-power of light intensity[26] (number of photons x photon energy)/(time x area) and the number of molecules in the cross-section. The cross-section is proportional to area, so the rate of OPA does not depend on light intensity. Means that the number of molecules excited by one-photon absorption is constant in any transverse plane of a focused laser beam inside the material.

On the contrary, the rate of MPA processes depend on light intensity as the relation between absorption and light intensity is nonlinear. In the case of TPA, the rate of absorption in a transverse cross-section of a laser beam is proportional to the intensity squared times to the number of molecules in the cross-section[30]. The absorption rate therefore scales inversely with area following a gaussian like distribution[31]. A TPA process is localized as it can only happens inside the focal volume of a laser beam where the light intensities could be large enough.

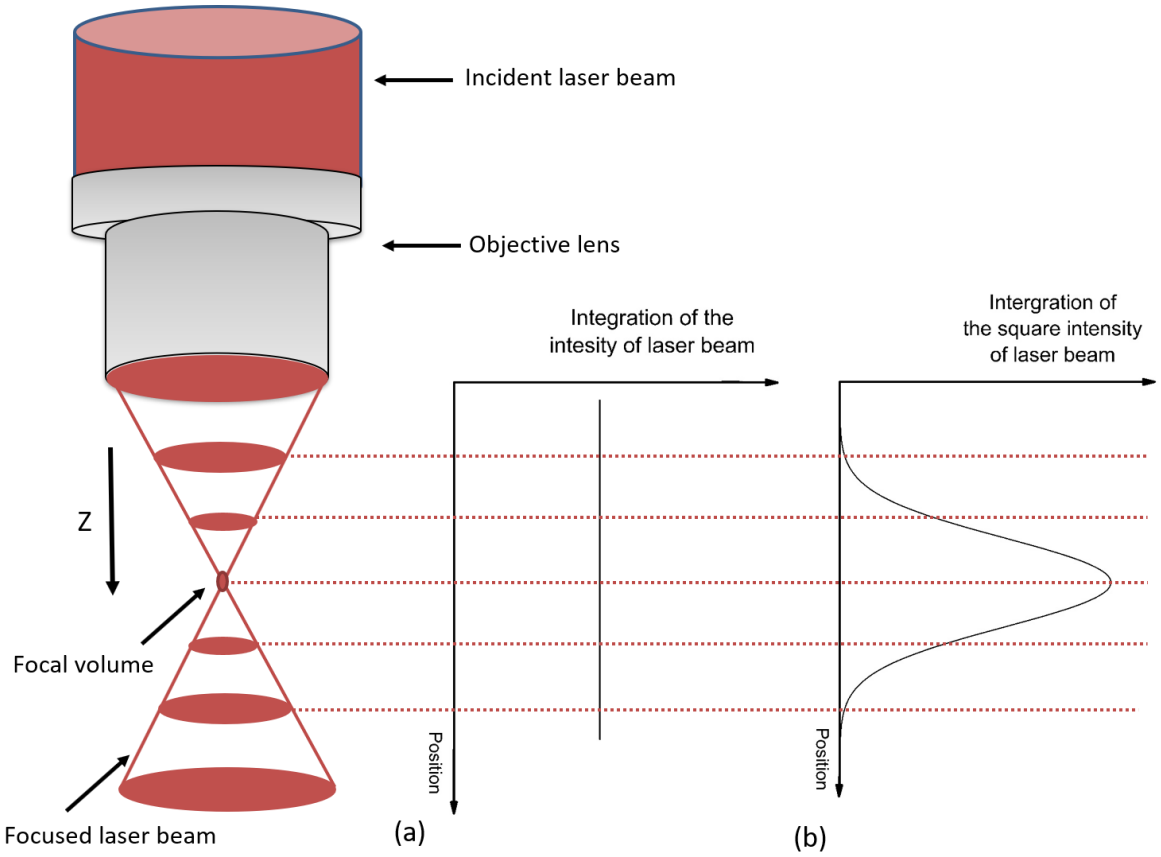

Figure 1.4: OPA rate (a) and TPA rate along the optical axe of a focused laser beam (b). In the case of TPA, the density of excited molecules will therefore be in the volume element in which the laser beam is focused most tightly. In comparison, in OPA there is no localization of excitation in the focal region.

Despite that the laser's characteristics and material's features were needed for MPA processes, the use of objectives lens is crucial for the process. Objective lens with high numerical aperture[32] (NA) is employed to focus the laser beam and create the photon density needed for nonlinear absorption. In order to have the greatest focus it is necessary to adjust properly the laser beam so that to overfill the back aperture of the objective lens as the beam comes through the objective.

In-volume patterning[1] and great fabrication's resolution are important benefits of the use of TPA, through which TPP induced. For the first one feature, materials were utilized for fabrication should have negligible absorption of the spectral region in which laser emits. Thus, the laser beam can penetrate deeply into materials and directly drive photopolymerization without contaminating outside of the focal volume. As indicated above, the second one feature is the spatial localization of TPA process which comes from the quadratic dependence of TPA rate on light intensity. As a result, the volume where TPA can occur is limited. Additionally, should taking into consideration the fact that high light intensities are required for TPA because that the two-photon transition rate is very small. Combining these with the use of an objective lens with high numerical aperture which can focus tightly the laser beam, there is capability to define a great accurate focal volume in which TPA occurs. By controlling and moving the focal volume of the laser beam through a transparent and photopolymerizable material, 3D structures can be fabricated by selectively inducing TPP of material which comes from TPA.

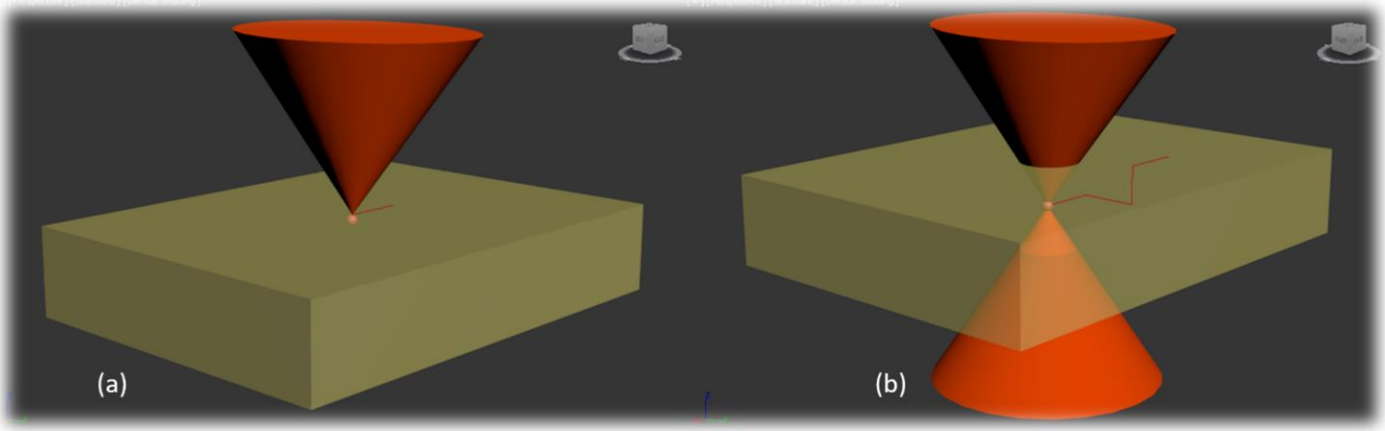

Figure 1.5: Schematic illustration of what can be caused from OPA or sequential TPA (a) and from simultaneous TPA (b) as laser beam focused in a photopolymerizable material by an objective lens. In the former cases, only processes close to the surface can be done. In contrast TPP, induced via simultaneous TPA, can be initiated only into the volume of a tightly focused laser

1.3 Two-photon polymerization

Polymerization is a process in which monomer molecules are connected with bonds to form polymer molecules. In the case of photopolymerization, light irradiation of a tightly focused laser beam provides the energy needed to drive the polymerization. Low weighting, photosensitive molecules can be added into material in order to increase the photopolymerization efficiency. Such as molecules called "*photoinitiators"* can absorb light irradiation and initiate the polymerization process through their excitation and decomposition.

In the case of TPP[30], photoinitiators are excited by absorbing simultaneously two photons with appropriate wavelength. As a result, active species are produced and the kind of polymerization is defined depending on active species. If active species are radicals, the polymerization is called "*free-radical photopolymerization*". This process includes chain reactions in which the addition of a monomer molecule to an active chain-end regenerates the active site at the chain-end. Thus, polymers can be formed by union of monomer molecules with bonds along a chain, with this way a phase transition could be accomplished.

Briefly, the TPP process can be described by the following steps[8]:

- Initiation: $I \xrightarrow{hv/2,\ hv/2} I^{*} \longrightarrow R^{\cdot}$
- Propagation: $R^{\cdot} + M \longrightarrow RM^{\cdot} \xrightarrow{M} RMM^{\cdot} \xrightarrow{M} \cdots\cdots \xrightarrow{M} RM_n^{\cdot}$
- Termination: $RM_n^{\cdot} + RM_m^{\cdot} \longrightarrow RM_{n+m}R$

The first essential step for photopolymerization is initiation, where radicals are produced via photoinitiators' excitation and decomposition. Therefore, during next step which is propagation a radical reacts with a monomer unit so that these are connected to form a first active monomer radical which can react with a new monomer unit and so on. Monomers continue to add in the same manner resulting in the formation of macroradicals, which are end-active polymers. In the final step called termination, chain propagation stops when two macroradicals meet each other so deactivation occurs with their connection.

The volume element inside material where polymerization occurs is defined as "*voxel*". In order to initiate photopolymerization of a material's molecules, the energy by absorbing light irradiation have to overcome a threshold energy which is defied by material used. As a result, TPP can take place only into the voxel and this feature can improve the fabrication's resolution. Taking into consideration, the benefits of TPA process combining with the existence of polymerization threshold leads to the conclusion that there is capability to control the fabrication process by knowing and modifying the incident light intensity and polymerization threshold.

Photopolymerization use light instead of heat to drive polymerization and this feature gives a crucial advantage. The electron excitation is occurred by a heat insulation process because of the incident photon energy is deposited much faster[33,34] than electrons could transfer it to the lattice through phonon emission.

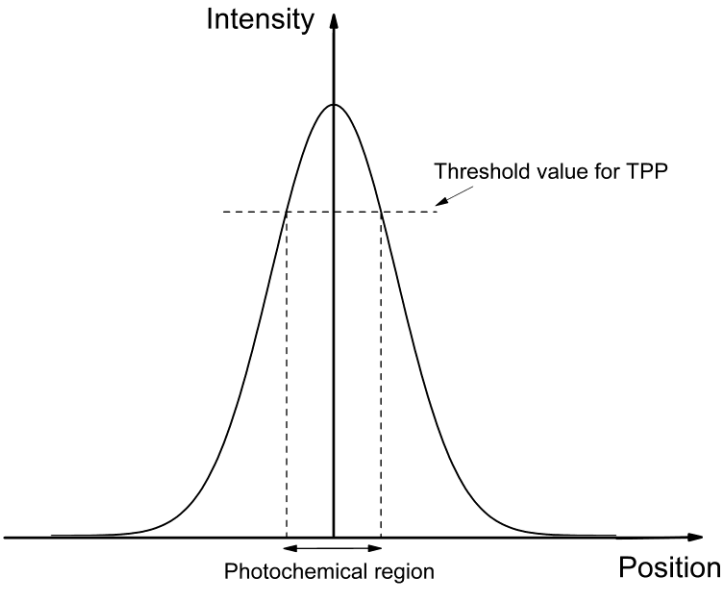

Figure 1.6: A diagram that shows the light intensity of a laser beam as it is focused by an objective lens along the position inside a material. TPP can take place only in volume where the light intensity is higher than the polymerization threshold of a material so the photochemical region is defined.

As referred above TPA process leads to TPP process so apparently by increasing TPA rate, TPP rate should be increasing. In contrast, there is a polymerization threshold and its existence imply that the incident light intensity should overcome a specific value so TPP takes place. The polymerization threshold, which depends on material used, comes from the fact that there are competitive processes[35] against polymerization. Initiation procedure can dominate these processes with the increase the number of radicals by increasing of light absorption. Therefore, voxel doesn't correspond to focal volume due to existence of a polymerization threshold which means that there is a minimum value of incident light intensity that can drive photopolymerization.

Theoretically, there is a natural limit on how much a light beam can be focused so the fabrication accuracy should be determined by this. The highest resolution that can be achieved by a focused laser beam is given by Abbe's diffraction limit[8]:

$$\text{Diffraction limit} = \frac{0{,}5\lambda}{\text{NA}}$$

where λ is the laser wavelength and NA is the numerical aperture of the objective lens.

Fortunately, the use of materials with well-defined polymerization threshold can provide voxels smaller than focused volumes and in this way the fabrication resolution can be achieved beyond the diffraction limit of light.

1.4 Materials

The idea is that the combination of two or more materials with different functionalities can give new hybrid materials with desire properties[36]. A way to accomplish that is to develop materials consisting of both organic and inorganic components. Advantage of these hybrid materials is that they represent good mechanical endurance and chemical stability from inorganic part and in addition great photosensitive effectiveness due to organic part. Pure inorganic or organic materials cannot achieve these properties. For the preparation of a hybrid material, the sol-gel process[37] can be used where formation of an inorganic network is achieved. Therefore, photopolymerizable functional groups from monomer units of the organic part are attached to the inorganic network. With addition of a photoinitiator, the MPA can be accomplished via interaction of photoinitiator with specific wavelength range of light irradiation. Thus, photoinitiators give photosensitivity to these hybrid materials[38].

The first step of the sol-gel method is hydrolysis and condensation where monomer units are mixed with water to form a porous interconnected cluster structure. Either an acid such as HCL or a base like NH_3 can be employed as a catalyst.

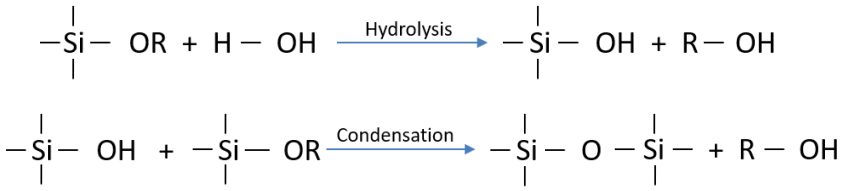

Figure 1.7: Chemical reactions between a silicon composite as organic monomer and a water molecule where the R groups are carbon chains. Through hydrolysis, a hydrogen atom replaces a R group of a monomer. Through condensation an inorganic network is formed.

The next step is gelation, where trapped water molecules are removed from the network. This can be done by drying the mixture at low temperature or low vacuum conditions for few hours. Hydrolysis and condensation procedure continue taking place in parallel with gelation procedure and so on while the mixture loses any significant volume at this point. So, formation of an inorganic network is achieved at the end of the process[39].

The hybrid material should have another important feature[8], they must be either negative or positive photoresist. In the case of negative photoresists, the absorption of light irradiation results in the cross-linking of the polymer chains, making the exposed area insoluble to an appropriate solvent used to remove the unpolymerized material. In order to produce the 3D substrates needed for this work, TPP method is implemented with negative photoresists as materials so the result is a direct laser writing technique of 3D structures in the sample material.

Differently, in the case of positive photoresists the reverse structure is written in the sample related to CAD design. Light absorption causes the photoresist's chains to break and become soluble to a convenient solvent so the unexposed area of the material stands.

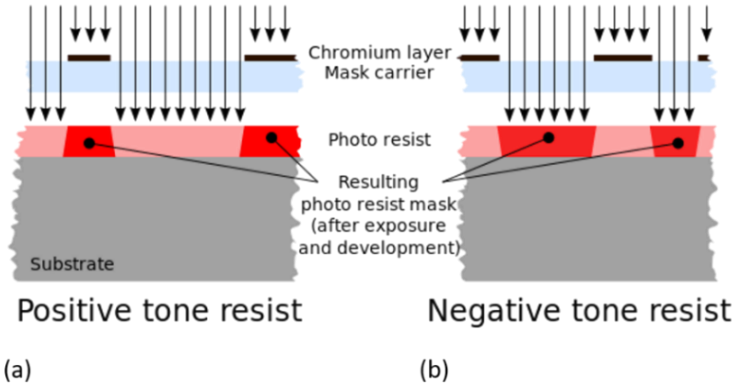

Figure 1.8: Schematic illustration of light irradiation exposure of a positive photoresist a) and a negative photoresist. This is an example of classical lithography where mask used in order to fabricate selectively the desire structure.

In this work, the materials which were utilized in order to produce the hybrid organic-inorganic material for MPF method is the Methacryloxy-Propyltrimethoxysilane (MAPTMS) and methacrylic acid (MAA) as organic monomers, zirconium propoxide (ZPO) for the formation of inorganic network and also 4,4'- Bis(diethylamino) benzophenone (BIS) as photoinitiator. All chemicals were purchased from Sigma-Aldrich.

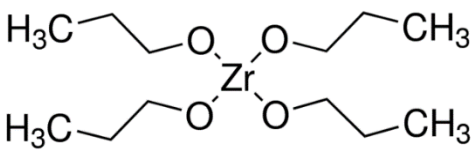

Zirconium propoxide (ZPO)

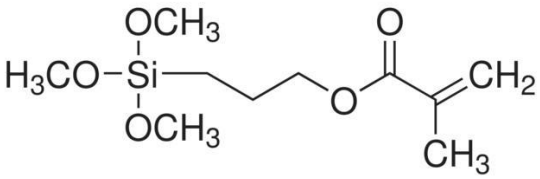

Methacryloxy-Propyltrimethoxysilane (MAPTMS)

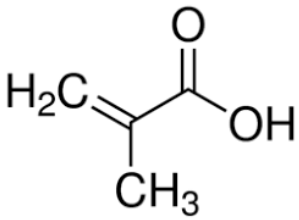

Methacrylic acid (MAA)

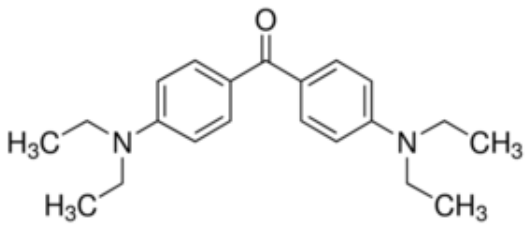

4,4'- Bis(diethylamino) benzophenone (BIS)

Figure 1.9: Structural formulas of the materials making the new hybrid material. The combination of these in specific concentrations result in the formation of an inorganic network which can carry photopolymerizable functional groups. After the polymerization of the organic part, a final organic-inorganic network will be arisen.

Material synthesis[40,41]: First, MAPTMS (7:3 molar ratio as to ZPO) is hydrolyzed in a flask with the addition of HCL at concertation 0,1M. The mixture is then stirred for 15 minutes until to become homogeneous. In a separate flask, we add ZPO and MAA in 1:1 molar ratio followed by stirring which is lasting 15 minutes. No reaction occurs between ZPO and MAA but MAA is used to protect ZPO from humidity as ZPO reacts with moisture. In the next step, the flask with MAPTMS is added to the solution of ZPO and MAA and another 15 minutes stirring is followed. At this point, solution undergoes condensation process in which the inorganic network is created. Another 5 minutes of stirring is followed after the addition of small amount of deionized water. Next, BIS is added to the mixture at 1% w/w related to the monomers and the solution is stirred for 15 minutes. In the final step, filtering process is necessary in order to remove large molecules from the solution and making it more homogeneous. Filters with a pore size 0,22μm are utilized for this purpose and after this treatment the hybrid material is then stored in 4℃ up to six months for future use.

Production of samples: The treatment of the hybrid material in order to use it in fabrication process deals with samples which are created by casting drops of sample material on a glass substrate. Firstly, the aim is that the glass substrates of samples have to be favorable for the fabricated structures by attaching them on their surface during writing. A way to achieve this is to spread out a thin layer of MAPTMS on the surface of the glass substrates. After immersing a glass substrate for 1 hour in the ultrasound machine in acetone, 1-propanol and ethanol sequentially, its surface is ready for treatment. A solution of 20mL dichloromethane and 250μL MAPTMS is added with an amount of glass substrates and the mixture is located in ultrasound machine for 4 hours. During this process, MAPTMS chains are created along a film layer on substrates' surface and then the glass substrates are ready to use. As referred above, a sample for fabrication is produced by casting drops of the material on a glass substrate. At this point, the gelation process is followed by drying the sample at low temperature (70℃) for an hour or by placing it at low vacuum conditions overnight.

After photopolymerization treatment: As described, during photopolymerization the radicals which are created, force chemicals bonds to break along the network. The fact that the polymerization occurs where the radicals are produced is favorable because in this way direct laser writing technique is achieved. According to the theory of negative photoresists, which described above, a process called "development" is followed after the photopolymerization. The role of this process is removing the unpolymerized material by immersing the sample for 15 minutes into a solution of 4methyl-2pentanone and 2-propanol with 1:1 volume ratio.

There is also a procedure called “wash” and its purpose is further cleaning 3D structures after the development. The way this process achieved is by immersing the sample into a solution of 2-propanol and deionized water with 7:3 volume ratio.

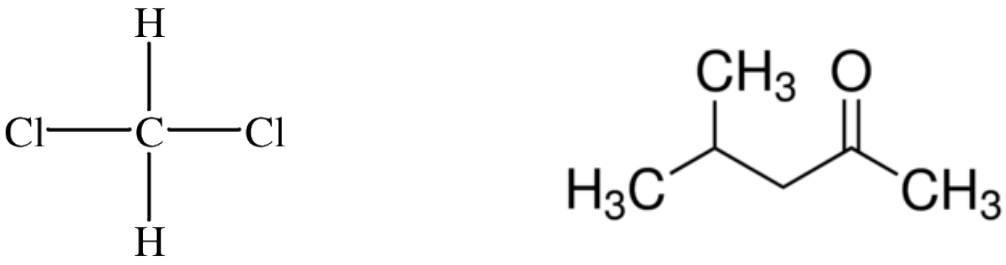

dichloromethane *4methyl-2pentanone*

Figure 1.10: Structural formulas of the solvents which are used for sample preparation and treatment before and after photopolymerization correspondingly.

1.5 Experimental set-up and process

The excitation source is a mode-locked Ti:Sapphire femtosecond laser operating at 800nm[42], which typically produces pulses with duration less than 200fs. Its repetition rate is around (50-80) MHz and its average output power can range from 200 to 600mWatts. With the use of a beam splitter, the laser beam is sharing into two paths called “Galvo” and “Nano” with 7:3 ratio respectively. As it is shown in the figure 1.12, series of mirrors are employed along the two set ups in order to direct the laser beam via optical components to the sample. There is beam control related to pass or not the laser beam to the rest experimental set-up. This is achieved by a mechanical shutter which is controlled by a computer for both “Galvo” and “Nano”. In addition, an attenuator is used to adjust the light intensity from laser beam which exposes the sample. This can be accomplished by corresponding angles from attenuator and light intensities from laser beam. Essential requirement for this match between angles and intensities is a powermeter through which the light intensity is measured. Thereby, there is capability to modify a desire incident light intensity to the sample by selecting an angle from attenuator via its connection with a computer. There is also a telescope system in order to adjust properly the laser beam size to overfill the back aperture of objective lens for better focusing conditions. Online monitoring of fabrication process is possible via a dichroic mirror and a CCD camera. The dichroic mirror reflects the incoming laser beam but allows green light from a led which illuminates the sample during fabrication process. In this way, information from illumination or light scattering is guided to the CCD camera which is connected with a computer.

Because of the difference on refractive index of light between the polymerized and the unpolymerized material, an image can be created in real time via a CCD camera. Through its connection to a computer there is capability for not only online monitoring but also controlling and modifying the fabrication process. At the end of optical path which leads to sample material, an objective lens is utilized (40x, NA=0,95, Zeiss, Plan Apochromat) and is located just before the sample in order to accomplish better focusing conditions.

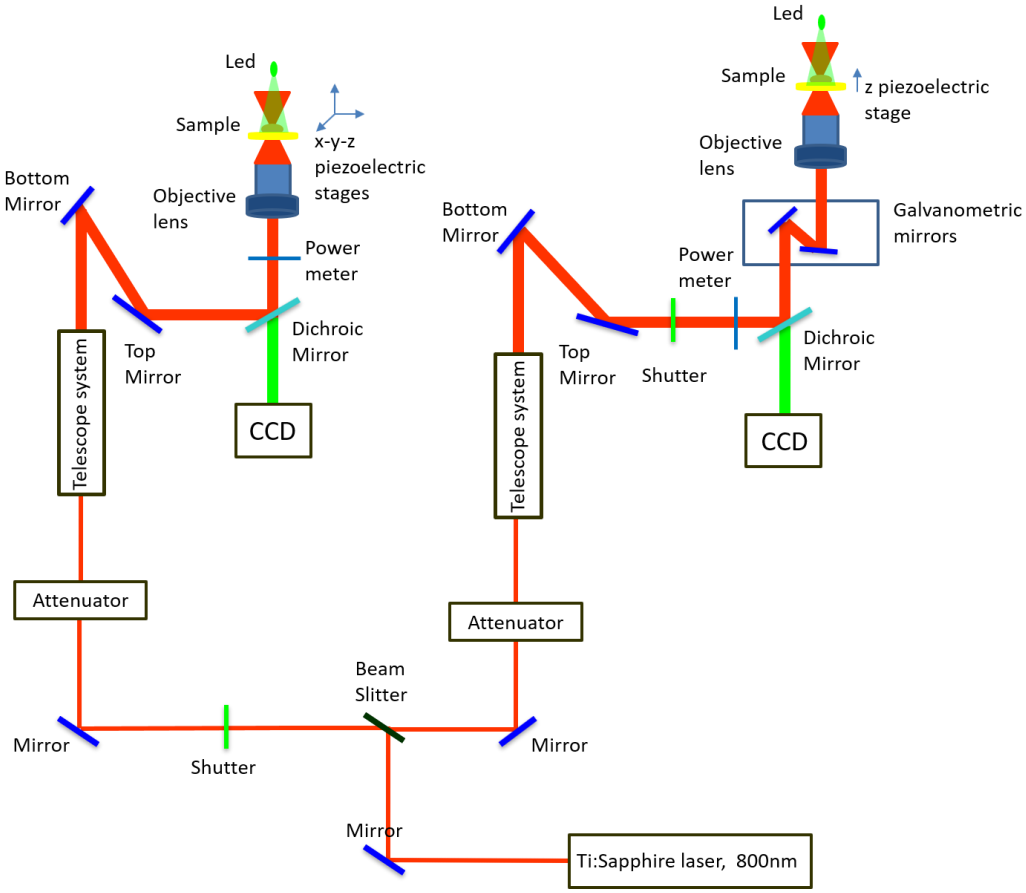

Figure 1.11: Schematic illustration of experimental set up which consists of two paths. It is shown the combination of optical components which were described above, making the set up favorable for direct laser writing of 3D structures.

The main difference between the two parts of experimental set-up is the way that fabrication occurs. In the case of "Nano", the sample is located on x-y-z piezoelectric stages. During structuring the laser beam remains immobile and the structures is generated by moving three-dimensionally of these stages. On the other side in "Galvo", the sample is located on a piezoelectric stage which moves only in z direction. Structuring layer per layer is achieved by laser beam scanning through x-y galvanometric mirrors, while sample remains immobile. One layer is first hardened according to the design pattern and then a new layer of the sample is added by the piezoelectric stage. The new patterned slice is polymerized and so on, thereby the entire structure is sequentially created by the same way.

Computer's system is connected with both two parts of experimental set-up, "Nano" and "Galvo" in order to control the fabrication process. Thus, there is capability to define the 3D design pattern with its dimensions through computers' software called "3DPoli" and "SamLight" in "Nano" and "Galvo" respectively. Through software there is also ability to modify fabrication parameters like: incident light intensity of the laser beam, exposure time by moving velocity of stages or mirrors respectively, and of course the estimated time of fabrication process. The aspect ratio of voxel is one of the most important parameters for fabrication of precise 3D microstructures. The combination of low laser power and long exposure time is advantageous to the formation of low aspect ratio voxels near the threshold energy[31]. This is the energy required for the polymerization process, it depends on material, photoinitiator and focusing conditions, but is usually in the order of a few nanojoules per pulse[43].

The sample is localized bottom up in order to avoid distortion of already photopolymerized material. Structuring starts from inside material according to the design pattern and finish with the structure's last features on a glass plate. After photopolymerization, the unpolymerized material is removed and the exposited pattern is remained on its glass substrate by immersing the sample material into an appropriate solution. So, the desire 3D structure stand. Although in this work, these structures are used as substrates for further treating.

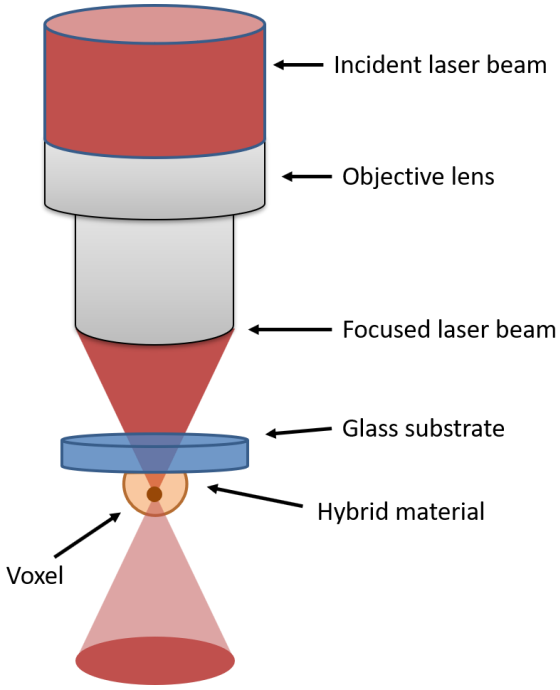

Figure 1.12: Visual illustration which shows how a laser beam is focusing from an objective lens to irradiates a sample. To avoid the distortion laser beam can cause to the built structures, the sample is localized bottom up.

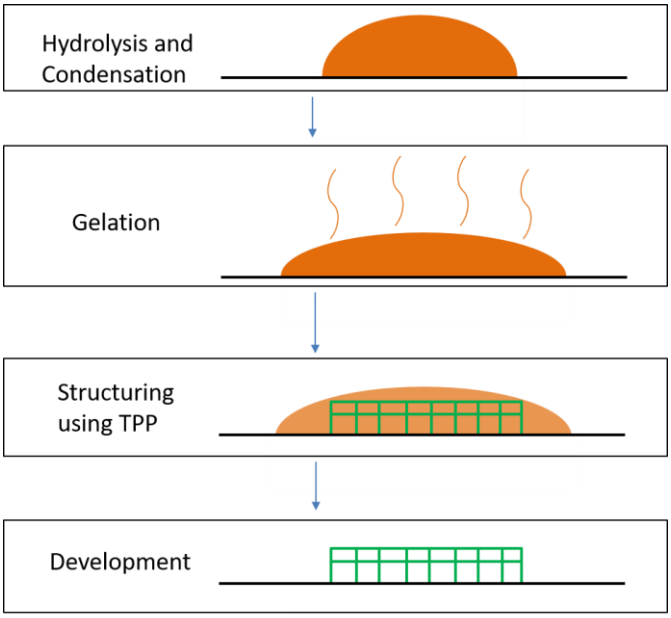

Figure 1.13: Processing flow of four steps, from sol-gel method, photopolymerization until further treating of the material, should be followed for direct laser writing technique

Chapter 2
Pulsed Laser Deposition

2.1 Introduction

PLD is a growth technique[44–47] of thin films, it is based on light interaction with a material in vacuum conditions. This method is achieved when a pulsed laser beam is introduced into a vacuum chamber through an optical window and focused onto a target material. There is light absorption by material and the result of this process was determined by the value of incident laser power density (energy/(surface x time)) related to an ablation threshold. For values of laser fluence (laser power density) lower than ablation threshold, laser pulse would simply heat the target. Ablation threshold depends on the target material, its absorption coefficient, the laser pulse wavelength and duration. Laser ablation and material vaporization of target occurs only if laser fluence is large enough to transcend the ablation threshold. In this case, a finite volume of solid target material converts into vapor phase constituents such as ions and neutrals, which form a high-temperature "plasma plume". Then ablation plume expands adiabatically transferring in this way vapors from target material to a substrate. Finally, recondensation of this plasma plume provide the material flux needed for film growth. A substrate is placed across to the target at a distance of few cm.

Laser ablation for thin film growth has many advantages against classical thermal growth techniques like chemical vapor deposition (CVD),[48] metalorganic chemical vapor deposition (MOCVD)[49] or ion-beam growth techniques like molecular beam epitaxy (MBE)[50]. In these cases, may be unable to accommodate all experimental components in the same chemical system because growth conditions needed for one can result in thermal decomposition of the other. In addition, may be unable to obtain the desire crystal purity on appropriate level or there might be limit on scale size of deposition area. While in PLD, laser is used as energy source of the process. It is localized outside of vacuum chamber away from the other components. In this way, a much greater degree of flexibility is providing for a variety[51–54] of materials can be used. Also, high crystal purity on film growth can be obtained because laser ablation and material deposition can be achieved by any solid phase material as target, no matter which is target material's kind or substrate's morphology. This is because material transferring on atomic scale, from target to substrate, is accomplished due to laser light absorption, plasma plume creation, expansion and recondensation. The most important feature of PLD method is the ability to produce thin films in the same element ratios of the any elemental components of the target material, even highly chemically complex targets due to plasma plume's nature.

2.2 Ablation mechanism

The mechanism of PLD technique apart from 4 stages[55,56]: laser light absorption by a target material, formation of a plasma plume, expansion of this plume and its recondensation for material deposition on a substrate for film growth. In the first stage, as laser beam irradiates target surface, light is absorbed by material according to Beer Lambert's law:

$$I = I_o e^{-\mu z}$$

where μ is the absorption coefficient, I_o is the incident laser light intensity, z is light distance through the medium, I is the laser light intensity at distance z inside the medium.

The absorption coefficient depends on medium, its temperature, wavelength and pulse duration of incident light irradiation. In general, the laser wavelength[57,58] and the laser pulse duration[59–62] are important parameters for the ablation process. Firstly, as decreasing the wavelength so energy increasing, the absorption coefficient is increasing. That is why laser sources, in UV spectral region, are more attractive because their use leads to high value of absorption coefficient. That means small interaction area between laser beam and target surface, so more effective light-material coupling. Moreover, light absorption cause excitation of material through electronic transitions. The energy of excitation is transferred by electrons to material's lattice through phonon emissions resulting in irradiated area's heating. During this stage, the temperature around the irradiated area rises up on the order of $\sim 10^4$K within a few picoseconds (ps). In the case of a fs laser-pulse, there is no laser-material lattice interaction because the pulse duration is shorter than the time required for plume development. Thereby, there is direct breaking of chemical bonds means that a phase transition is induced from solid to the vapor phase omitting the liquid one avoiding thermal effects. With fs laser pulse, the photon energy is deposited much faster than electrons could transfer it to the lattice through phonon emission as referred, so thermal effects are avoided. A typical laser source for ablation is a KrF excimer laser with pulse duration few tens of nanoseconds (ns) and pulse wavelength in UV spectral region. Big laser power output can be accomplished with this laser because it can provide great amounts of energy in short time making it favorable for laser ablation. As in this way, chemical bonds breaking is achieved, resulting in vaporizing of target material. Also, a well-defined laser beam profile is provided by a KrF excimer laser because such a profile is homogeneous and hence the energy distribution in a laser plume becomes also well-defined.

The second stage consists of target material vaporization and plasma formation. If incident energy per time per area from laser beam (laser fluence) overcomes an ablation threshold, species in the irradiated area are ejected from target material creating the characteristic plasma plume. Plume apart from ionized matter which consists of ground- and excited-state neutral atoms, electrons that are came from the chemical bonds breaking of the ablated material. During multiphoton ionization of the target surface, these ejected species continually absorb the incident laser light resulting in a strong interaction between the plume and the laser beam as well as the reheating of plume. The amount of evaporated material is localized only to that area defined by the laser focus and ejected atoms, molecules, electrons, ions, clusters and micron-sized particulates flow away from the target surface to the substrate at high mass transport velocity. The kinetic energy of plume species is on the order of few tens of eV. Laser parameters[63–66] such as laser fluence, wavelength, pulse repetition rate and pulse duration can affect the kinetic energy, flux and ionization degree of ablated species.

The third stage involves the plasma plume expansion in vacuum, after the laser pulse. The plume expansion is considered as adiabatic, because there is no mass or energy transfer to the ablation plume. As plasma expands adiabatically, it cools to temperatures typically on the order of 10^3K as expected due to volume increasing. Because of temperature decreasing, the kinetic energy of plasma species is decreased too on the order of few eV.

The final stage is the film growth of ablation material. Ion-electron recombination of the plasma plume is occurred, providing the material flux needed for film growth. During ablation and material transfer by the plasma plume, the deposition of the material to substrate is nonuniform due to the highly forward-directed nature of the plume. Scanning of the ablation beam over a rotating target could lead to more uniform film coverage of the desire material over substrate. The thickness[67] of the deposited film on the substrate is strongly dependent on the chamber pressure. That is to be expected because higher pressure (lower-vacuum) means more atoms and molecules inside the chamber. Those particles collide with the ablated atoms of the target, scattering them and reducing the total amount of ablated material reaching the sample. The process occurs under vacuum conditions around 10^{-6} mbar for this reason. In addition, the distance between target material and substrate plays a dominant role in thickness of thin film. Film thickness is inversely proportional to distance, so with an appropriate adjustment of distance, not only large areas[68] can be deposited homogeneously, but it is a way to produce the desire thickness. Also, pulsed nature of PLD means that film growth rates may be controlled, by repetition rate adjustment, to any desired amount adding a parameter for film thickness. Substrate temperature is another important parameter as it affects the diffusion length of plume species during deposition.

When PLD method is performed in the presence of ambient background gas[69–72] in combination with vacuum conditions, two effects are expected. The first one is the reduction of the kinetic energy of the vapor flux. The other one is the production of molecular species in the ablation plume by interaction of ablated species with the background gas effecting the material composition on film growth. Under typical conditions, the deposition rate per laser pulse can range from 0,001 to 1Å per pulse.

The feature, as refereed above, that makes PLD technique more attractive than others deposition techniques, is the capability of stoichiometric transfer of desire material from a target to a substrate. This can be done independently the kind of target and substrate[73,74] because PLD is based on a plasma plume. Plume apart from ionized matter, which is expand out from a target and flow toward to a substrate. Thus, material transfer is achieved on atomic scale, which leads to two benefits. The first one is that the phase of the target does not need to be the same as that of the desired film. The other one is that growth film can be accomplished on any kind of the substrate making the technique appropriate for material deposition on complex geometries[75,76] except of plane surfaces.

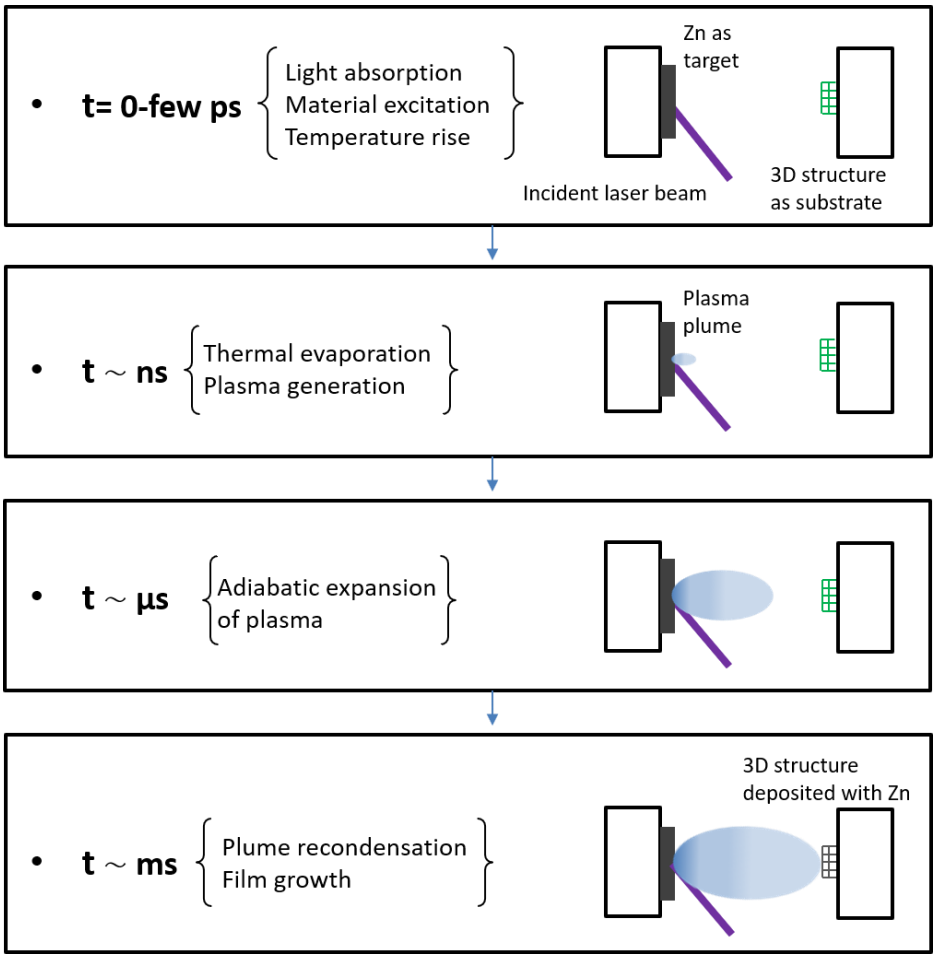

Figure 2.1: Processing flow of PLD process and approximate time scales during laser ablation. and plume propagation are shown in. A bulk pellet of Zn is used as target material and a 3D nest, which is fabricated via MPL, is employed as substrate.

2.3 Experimental setup and process[76,77]

The energy source is a KrF excimer laser operating at 248nm and its pulse's duration last 30 nanoseconds (ns). There is capability to adjust its repetition rate as well as its operating voltage. As it is shown in the figure 2.2, a set of mirrors is used in order to guide the laser beam to a vacuum chamber. There is a spherical lens (f=+30cm) before the chamber, with aim to focus the laser beam into a spot irradiating the target. A powermeter is utilized to measure the laser beam energy just before the chamber, thereby the error from the measurement is minimized. The laser beam is introduced to vacuum chamber through an optical window and a quartz glass which allows only light from the laser beam to pass. The chamber comprises a vacuum pumping system, a vacuum gauge, a rotating target holder and a substrate holder. The pumping system consists of a mechanical pump which is employed to create a preliminary low-vacuum on the order of 10^{-2} mbar and a turbomolecular pump which is activated at this point in order to reach the pressure on the order of 10^{-6} mbar. These vacuum conditions are essential for plume propagation and pure film growth.

The check of the vacuum conditions is done by a Pirani and a Penning gauge. Pressure measurements are achieved between (10^{3}-10^{-3}) mbar with the use of the first one gauge and between (10^{-3}-10^{-8}) mbar with the latter one. A bulk pellet of Zinc (Zinc foil 99,95%. GoodFellow) is used as target material and a 3D microstructure, which was prepared via MPF method, is employed as substrate sample. The target was rotated during laser ablation of material because it is a way to minimize crater formation. There are also optical windows along the vacuum chamber so PLD process can be observed. In conventional PLD experiments, pressure of an ambient gas within the chamber as well as substrate temperature are two crucial parameters to the process but in this work, they are not investigated.

The first step for the preparation of PLD process is alignment of the beam's optical path so as to laser beam irradiates the target material. In this way, there is capability to calculate laser spot size at target by irradiating with one pulse a photosensitive paper instead. The profile of the laser spot size is captured into the paper, so its dimensions can be measured. The 3D structure is placed on the substrate holder a target-to-substrate distance of 4cm at an angle of 45° with respect to the target surface and the vacuum chamber is sealed. With the use of the pumping system as well as the vacuum gauge which are described above the desire vacuum conditions are obtained. At this point, the laser beam energy is measured by powermeter. As the spot size of the laser beam was measured latter, there is ability to calculate the laser fluence (energy/surface), so through laser beam's energy adjustment there is ability to make the fluence to fit the desire value. The repetition rate is adjusted at 10Hz and the motor is activated, via which the target holder is rotating. The rotation speed of the target as well as the target-to-substrate distance are remained constant for all depositions in this work.

The number of pulses on the target throughout the experiment can be adjusted, either by the repetition rate or the total time of the deposition:

$$\text{total time (s)} = \frac{\text{number of pulses}}{\text{repetition rate (Hz)}}$$

So, the laser ablation and film growth can be done, after ending this procedure both pumps are isolated from the chamber and turned off. The chamber is opened and the 3D structure deposited with a thin film of Zn through PLD technique, is obtained.

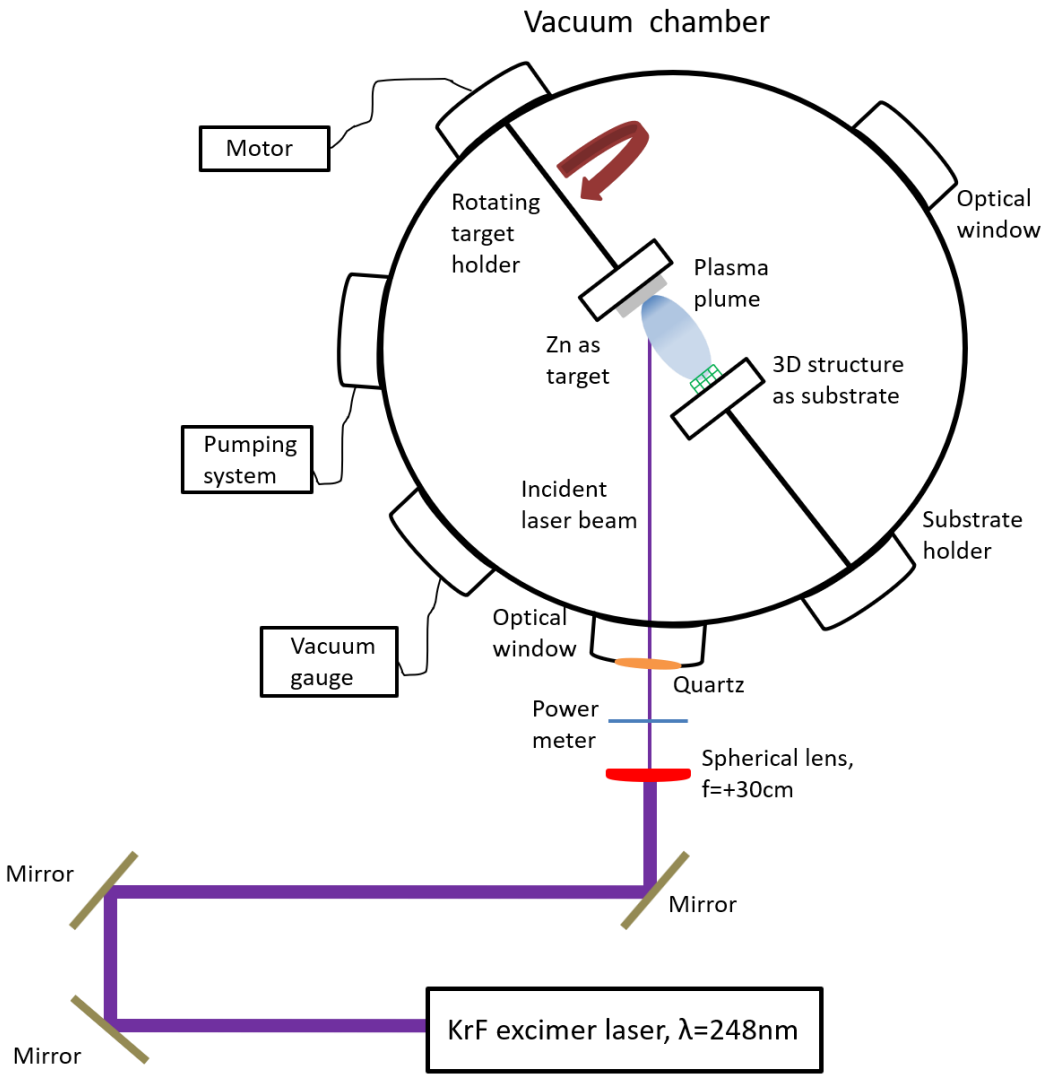

Figure 2.2: Schematic illustration of PLD experimental set-up which is used in this work. It is a standard PLD apparatus which is described above with aim the deposition of Zn thin film layer on 3D polymeric scaffolds.

Chapter 3
ZnO nanorods

3.1 Introduction

Zinc oxide[78] (ZnO) is a well-studied material due to its unique electrical, optical, catalytic and optoelectronic properties[79]. It finds use in a broad range of nowadays technology such as: gas sensors[80–84] and piezoelectric devices[85], UV light detectors[86,87], energy applications (batteries[88], solar cells[89,90], water splitting[91,92]), photocatalytic[93,94] and biological research[95–97]. ZnO is an II-VI direct gap semiconductor with a wide bandgap (3,37 eV) at room temperature and large exciton binding energy (60meV). ZnO crystallizes in the wurtzite structure, which is a hexagonal unit cell with lattice parameters "α" and "c" in the ratio of $c/a = \sqrt{8/3} = 1{,}633$. In wurtzite structure each zinc atom is surrounded by four oxygen atoms, which are located at the corners of a nearly regular tetrahedron. Due to its structure, this material presents a strong piezoelectric effect as there is conversion from mechanical energy into electrical energy. Melting point of ZnO is 1975℃ and its crystal lattice density is $5{,}67\ g/cm^3$.

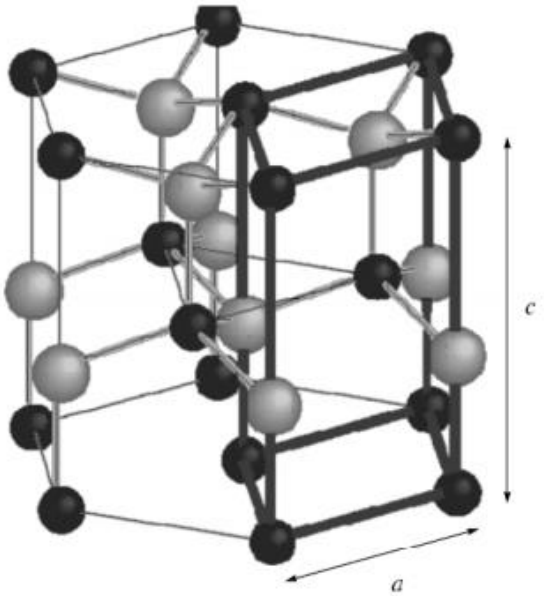

Figure 3.1: Schematic illustration where hexagonal prism of wurtzite structure of ZnO is shown. Black and white spheres denote Zn and O atoms, respectively.

Photoluminescence (PL) spectroscopy is a powerful optical method with aim to investigate the electronic structure of materials by giving information about their energy levels. During this process, laser light is directed onto a sample where it is absorbed impacting enough energy for electron transitions. This spectroscopy method is most common in semiconductor systems, where the excitation energy should transcend the energy difference between conduction and valence bands, with the energy difference being known as "bandgap". An electron excitation on conduction band generates a hole on valence band. The spontaneous process of electron-hole recombination induces light emission with energy of semiconductor's bandgap. Therefore, PL emission of ZnO[98,99] originates from its bandgap energy, which corresponds to a wavelength on UV spectral region ($\lambda \sim 370$nm).

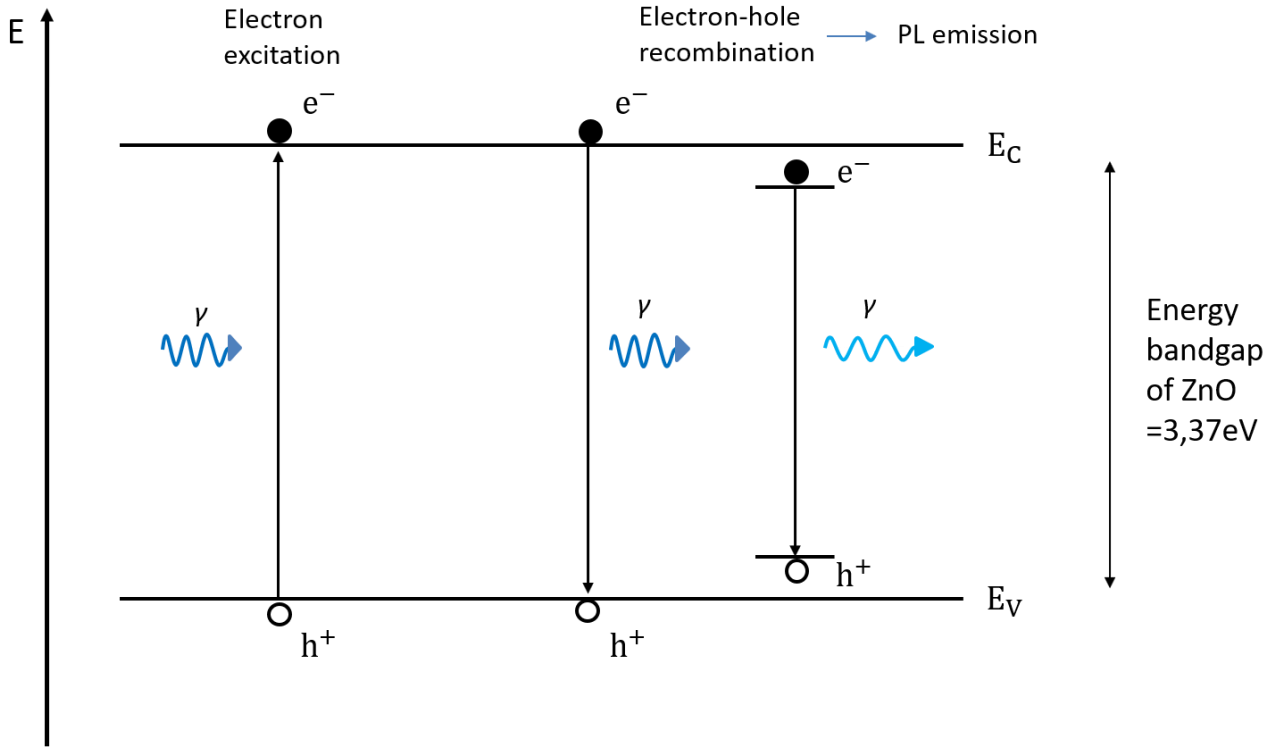

Figure 3.2: Schematic illustration of procedures leading to PL emission. Impurities in material's crystal lattice are responsible for reduction on light wavelength emission.

Doping of ZnO with other elements leads to an increase in the bandgap width as well as to an increase in the activation energy of donors. As a result, doping of ZnO with specific materials[100–102] can enhance the desire properties and use these compounds in various applications.

3.2 Aqueous chemical growth

Nanostructured materials[103] are expected to exhibit improved properties as compared with bulk materials due to large ratios of surface area to volume. As a result, the growth of nanostructures has attracted a lot of interest in nowadays research. Aqueous chemical growth (ACG)[104,105] is a solution growth technique, which is a quite simple method for growth of nanostructures of various materials[106,107]. It is taken place at relatively low temperatures, presenting several advantages such as the use of non-expensive equipment, the requirement of cheap and non-toxic reagents and the presence of non-hazardous by-products. ACG's big advantages against other growth techniques[108] such as: physical vapor deposition (PVD) and vapor liquid solid (VLS), is the large scale of development area combining the fact that low temperatures are needed. It is also a simple and controllable solution method for growth of ZnO nanorods.

Materials: All the chemicals, used in this point of work, were purchased from Sigma-Aldrich. Zinc nitrate hexahydrate ($Zn(NO_3)_2 \cdot 6H_2O$, 98%) and ammonium hydroxide solution in water (28 wt% NH_3 in H_2O). Growth solution was prepared by dissolving a calculated amount of zinc nitrate hexahydrate in 80mL of deionized water to make a 0,02M solution. Ammonia water was added to adjust the pH of the growth solution. The amount of the added ammonia water was 2,5mL. As referred, a Zn thin film, which is deposited on 3D structures, is a crucial parameter for growth of ZnO nanorods since it is employed as a seed layer to improve the uniform alignment of nanorods on 3D substrates. The thickness of zinc layer was also an important feature, around 100nm in this work. $Zn(NO_3)_2$ acted as a source of zinc ions (Zn^+) and ammonium solution was used to supply (OH^-) to assist the reaction. The role of initial zinc seed layer is shown in this point, since metal Zn works as precursor and direct the nucleation process for ZnO molecules. Following reactions are occurred for synthesizing ZnO nanorods:

$$NH_3 + H_2O \rightarrow NH_4^+ + OH^-$$

$$Zn^{2+} + NH_3 \rightarrow Zn(NO_3)_4^{2+}$$

$$Zn(NO_3)_4^{2+} + 4OH^- \rightarrow Zn(NO_3)_4^{2-} + 4NH_3$$

$$Zn(NO_3)_4^{2-} \rightarrow ZnO_{(s)} + H_2O + 2OH^-$$

ZnO nanorods characteristics:

The nature of wurtzite structure advantages the development of ZnO nanorods along c-axes[109], since the Zn-O atoms spacing is slightly shorter along the c axis than that of the other Zn–O bonds in different directions.

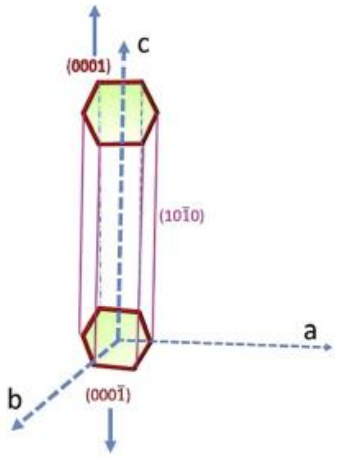

Figure 3.4: Visual illustration of alignment of ZnO nanorods along c-axes

Morphological and structural characteristics, aspect ratio[110] or shape[111] for example, of grown nanostructures can be controlled by adjusted parameters such as: pH[112,113] of solution, growth time[114] of procedure and substrate[115–117] for nanostructures. As referred, the role of seed layer of Zn thin film, is to direct the growth of ZnO nanorods by providing Zn ions where the reactions can occur.

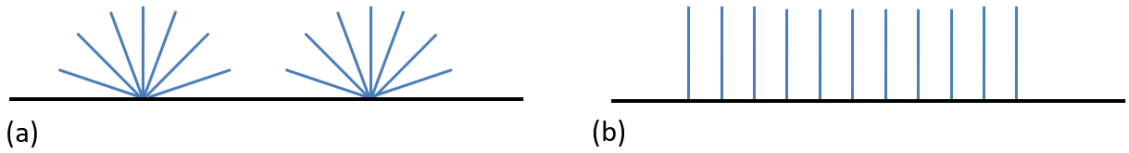

Figure 3.5: Visual illustration of ZnO nanorods grown on flat substrates by ACG. a) the result of ZnO nanorods growth without seed layer of Zn, b) the result of ZnO nanorods growth with seed layer of Zn by PLD technique.

Process:[118,119]

Hydrothermally ZnO nanorods growth was carried out by suspending the 3D structures deposited with zinc, bottom up in a glass bottle filled with the growth solution. The growth temperature was selected 95℃ and growth time ranges from 1,5 to 3 hours. After growth, the samples were removed from the solution and were immersed for 15 minutes in a solution of deionized water and ethanol with 7:3 volume ratio respectively. Then, drying in air is followed for another 15 minutes.

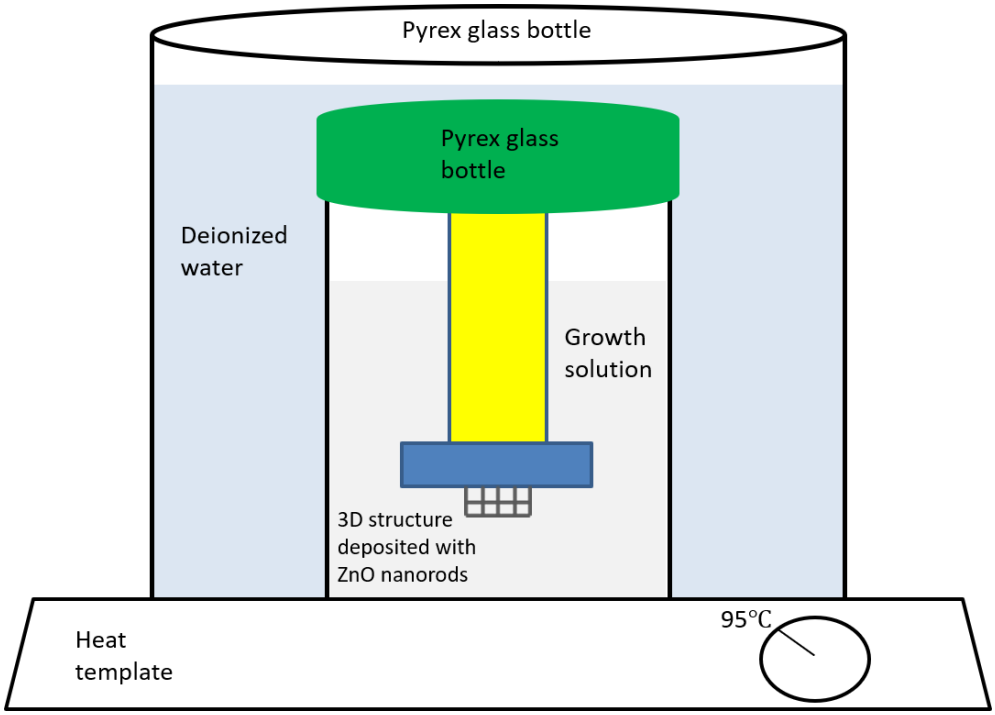

Figure 3.3: Schematic illustration of experimental set-up of ACG. The 3D structures are localized bottom-up in growth solution in order to form ZnO nanorods on them without gravitational effects.

Chapter 4
Results

4.1 3D substrates

3D structures which were fabricated via MPL method, are shown in this chapter via Scanning electron microscopy (SEM) images.

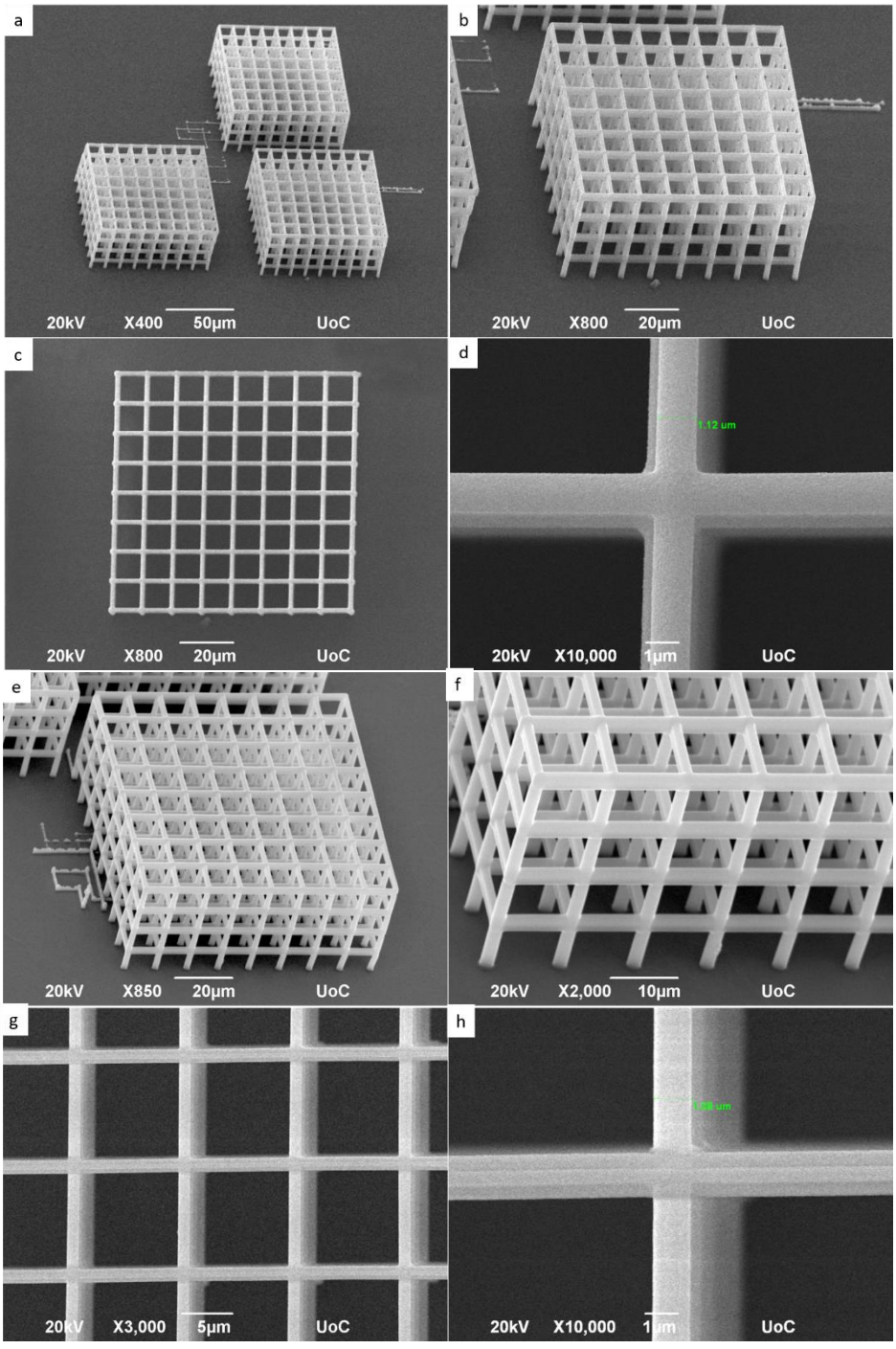

Figure 4.1: SEM images of a 3D structure which is called 3D grid, a) three 3D grids, b),c),e) zoom in one of three, f),g) further zoom in d),h) fabrication resolution ~1-1,10μm.

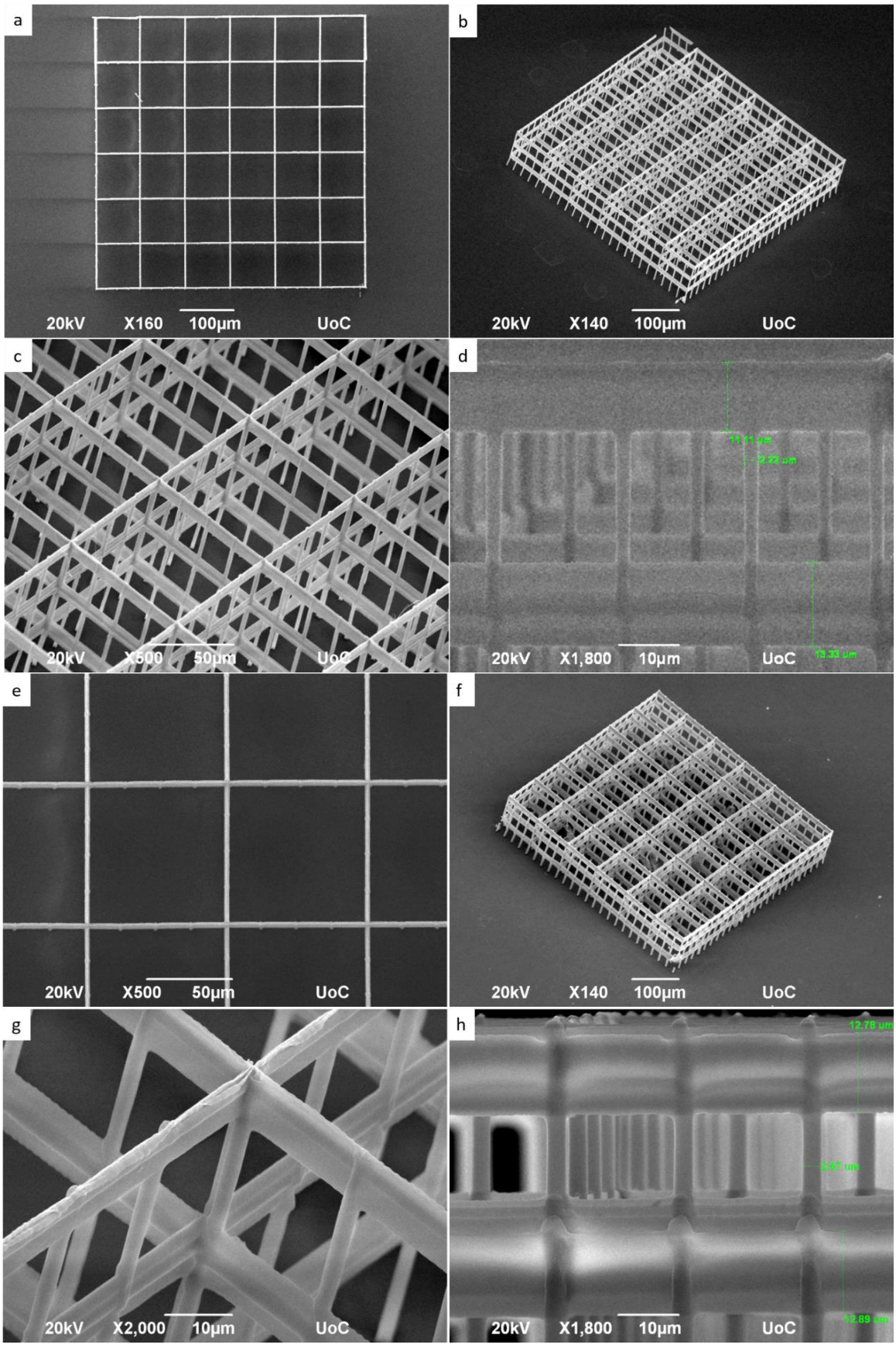

Figure 4.2: SEM images of a 3D structure which is called 3D nest, a) top view, b),f) tilted view, c),f),g) different zoom in nests d),h) fabrication resolution ~2,5µm and ~12µm in x and y directions respectively.

The hybrid material as well as the sol-gel process, which were employed in order to fabricate these structures, were described on the chapter of material in MPL method. In addition, the rest experimental parameters of fabrication process for this structure are: laser power = 10mW, fabrication velocity = 20μm/s for 3D grid and laser power = 21mW, fabrication velocity = 40μm/s for 3D nest. 3D grid's dimensions are: (80x80x40)μm^3 and 3D nest's dimensions are: (480x480x60)μm^3.

4.2 3D structures with aligned ZnO nanorods

The process followed in order to synthesize ZnO nanorods on 3D structures is a typical ACG process. Concentrations of materials used are referred above. The growth temperature was selected 95℃ and growth time ranges from 1 to 3 hours. The diameters of the nanorods ranged from 0,5 to 1 μm and their length ranged from 1 to 3μm.

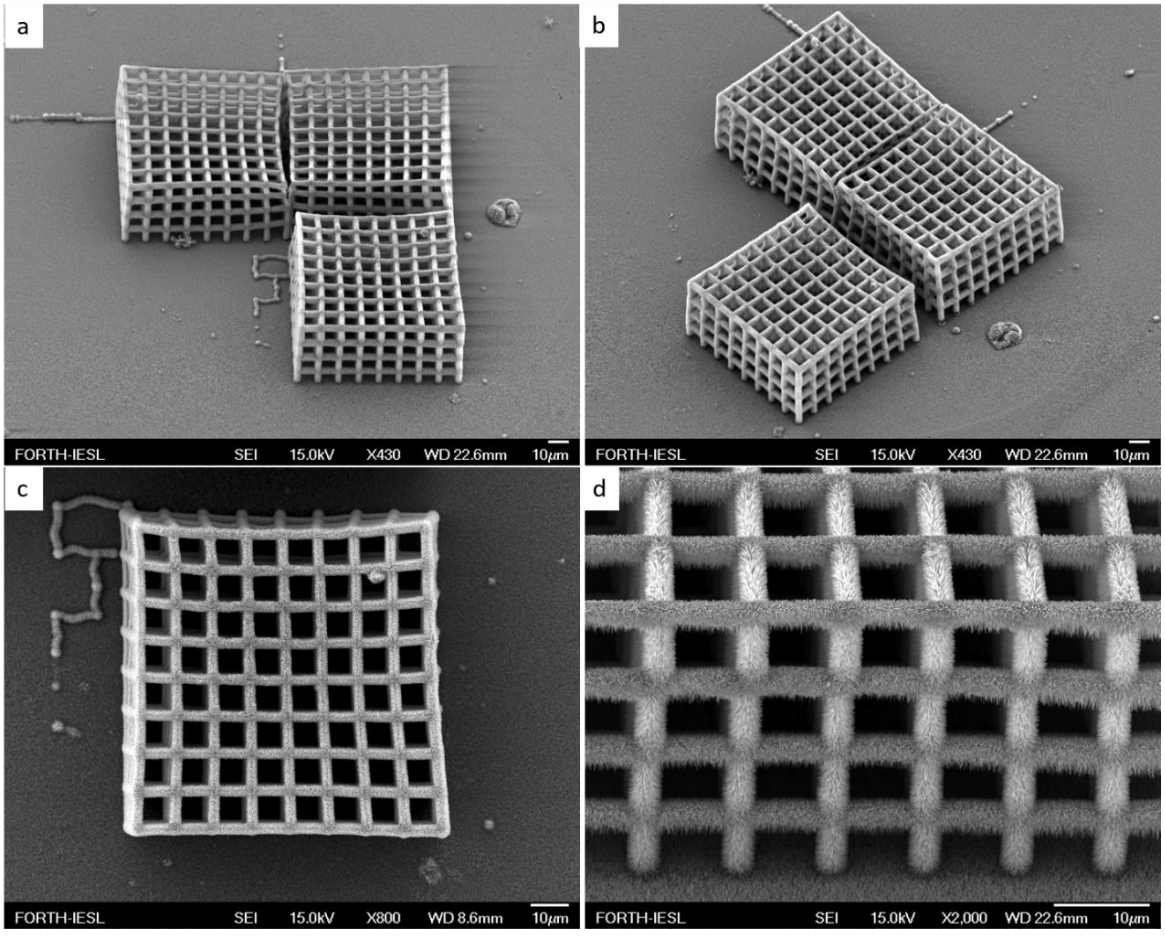

Figure 4.3: SEM images of 3D grids deposited with ZnO nanorods and with growth time 2,5 hours, a),b) three of 3D grids, c),d) zoom in one of them as they are fabricated with same experimental parameters.

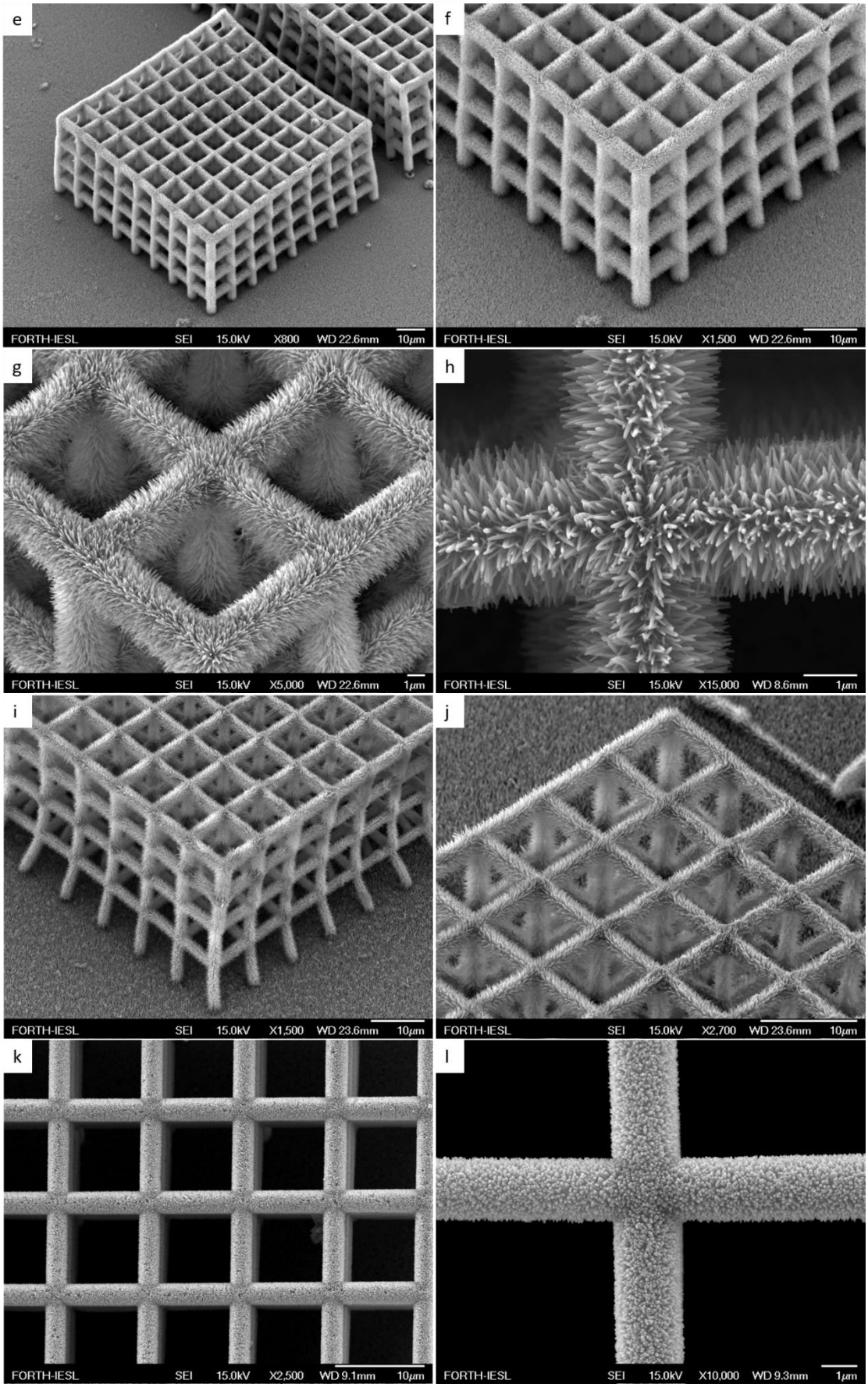

Figure 4.4: SEM images of 3D grids deposited with ZnO nanorods, e),f) growth time 2 hours, g),h) growth time 2,5 hours, i),j) growth time 3 hours, k),l) growth time 1 hours.

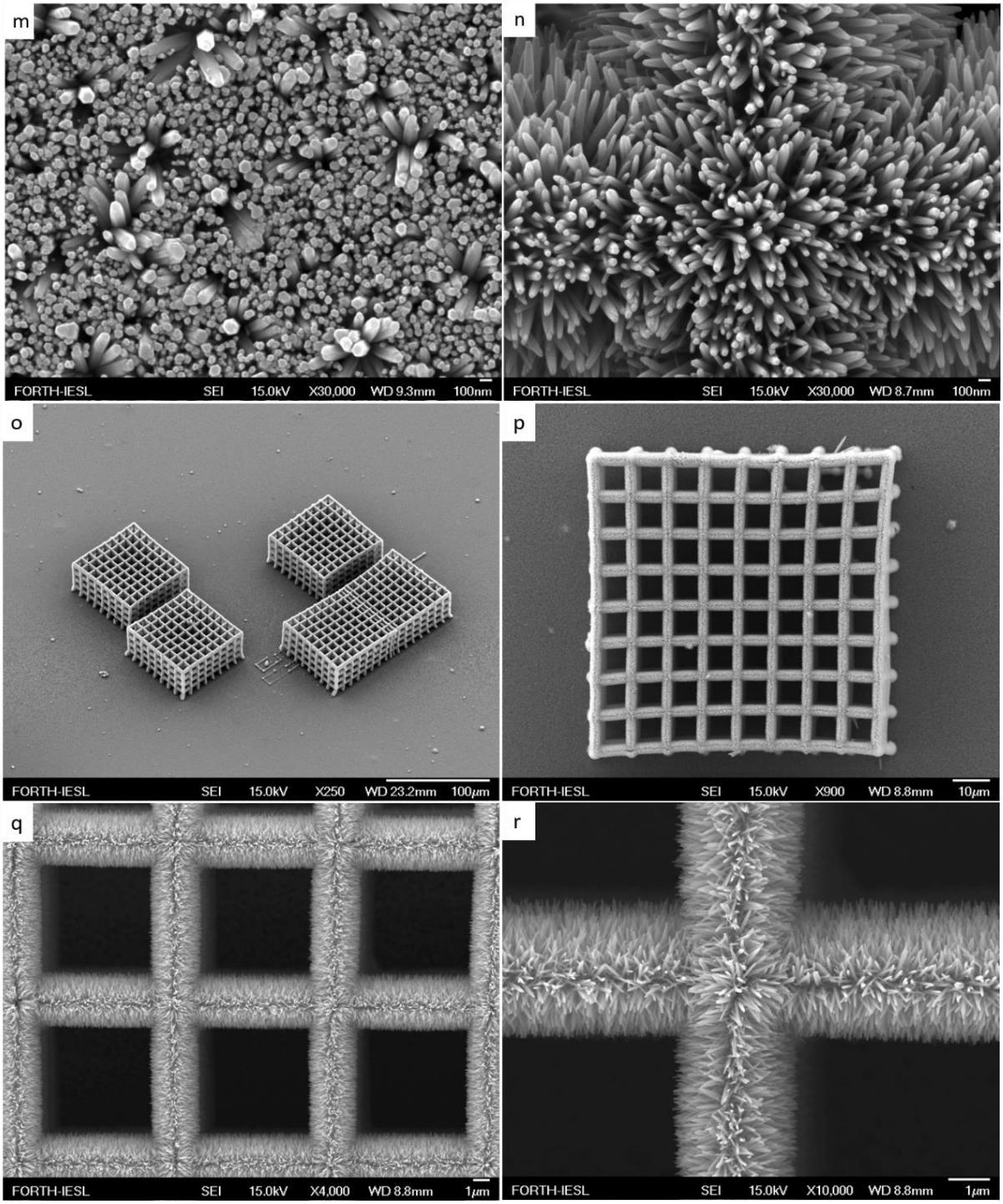

Figure 4.5: SEM images of ZnO nanorods with growth time 2 hours, o) 3D grids deposited with ZnO nanorods, p),q),r) zoom in one of them, m) ZnO nanorods on a flat substrate, n) ZnO nanorods on a 3D substrate.

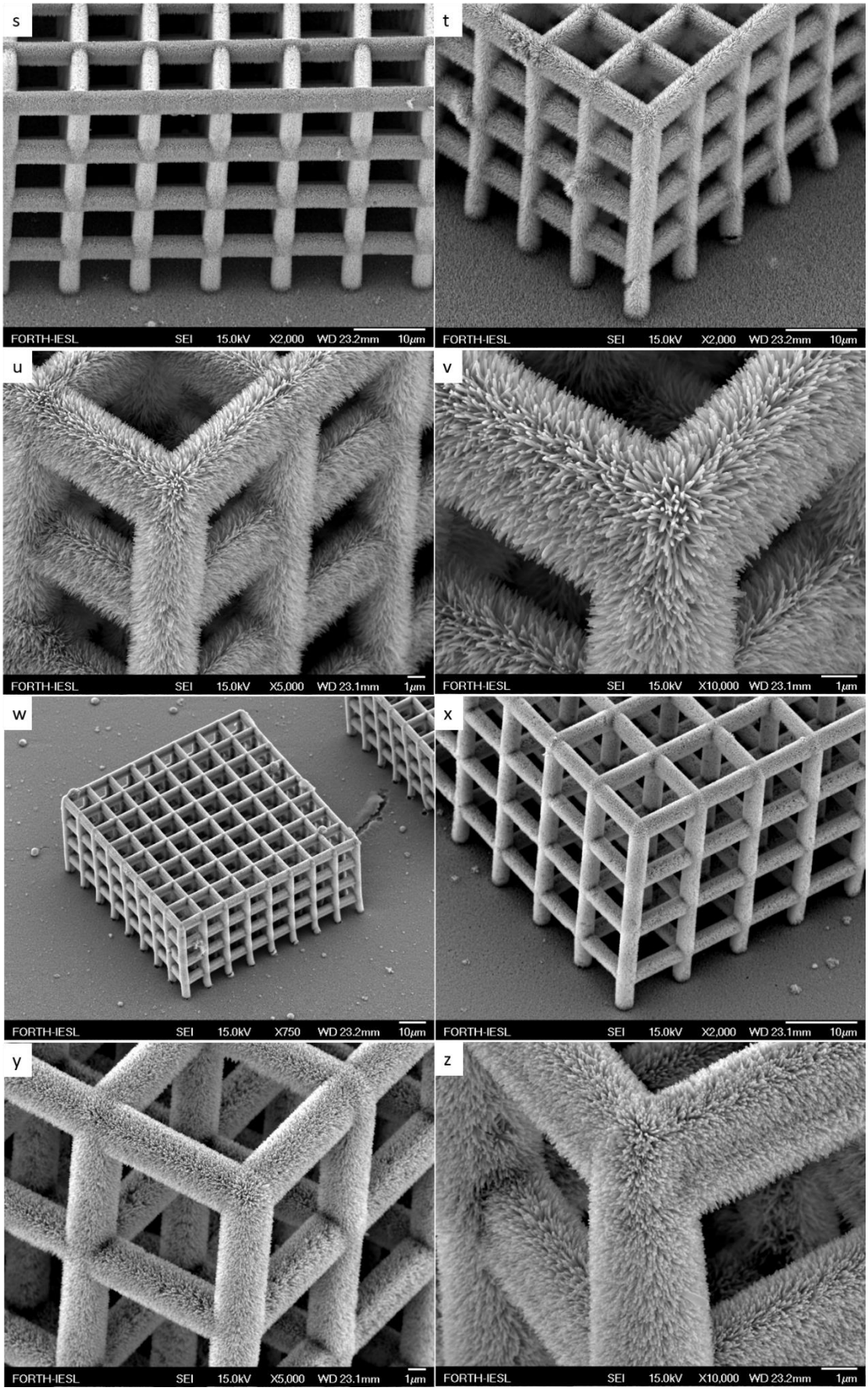

Figure 4.6: SEM images of 3D grids deposited with ZnO nanorods, s),t),u),v) zoom in a structure with ZnO nanorods and with growth time 2,5 hours, w),x),y)z) zoom in a structure with ZnO nanorods with growth time 2 hours.

4.3 Photoluminescence measurements

Photoluminescence measurements of 3D structures consist of ZnO nanorods were carried out by using a 248nm wavelength KrF laser as excitation source.

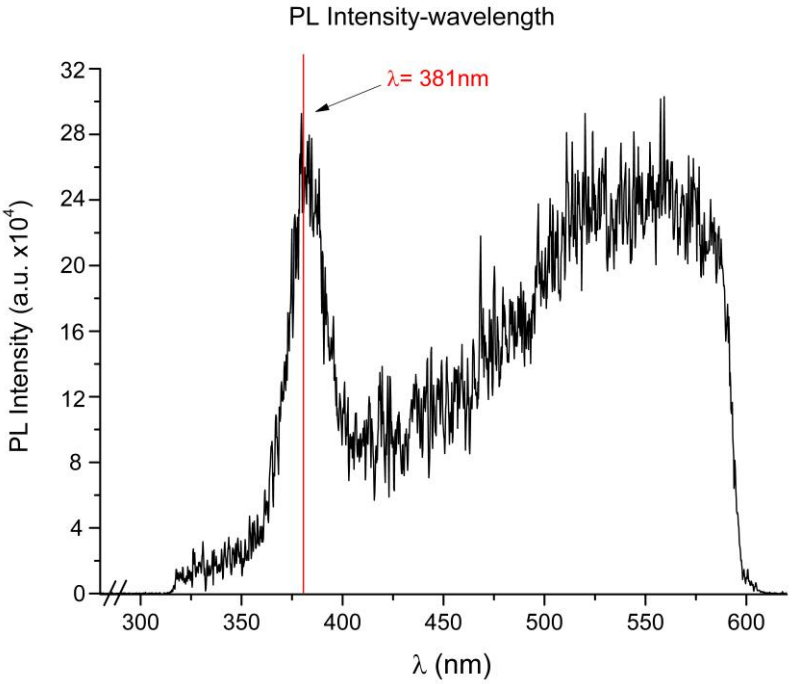

Figure 4.7: Diagram of PL intensity related to wavelength on sample of a 3D nest deposited with ZnO nanorods but on flat area. PL peek is centered at 381nm as expected due to ZnO bandgap energy. Impurities in crystal lattice are responsible for increase on light wavelength emission.

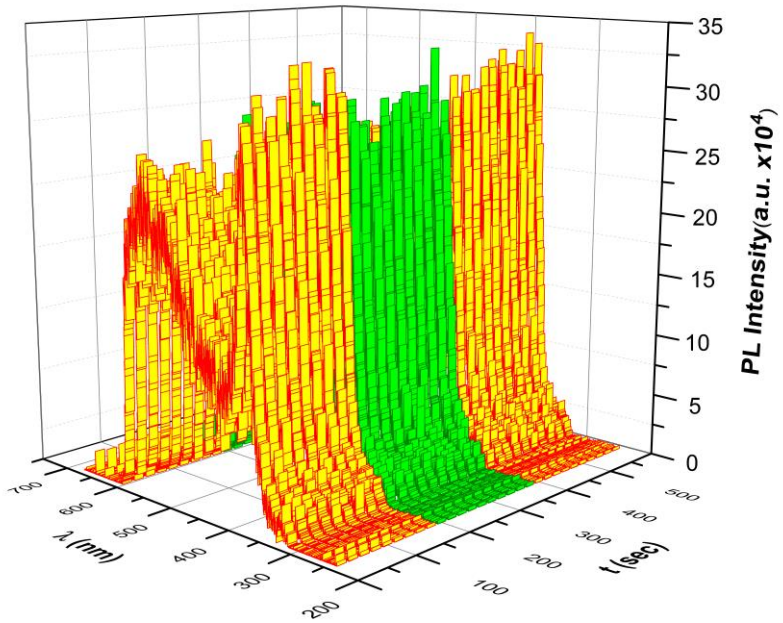

Figure 4.8: Diagram of PL intensities related to wavelength and time on sample of a 3D nest deposited with ZnO nanorods but on flat area. There was change in the environment of 3D nest, yellow measurements represent vacuum environment and green measurements represent air environment.

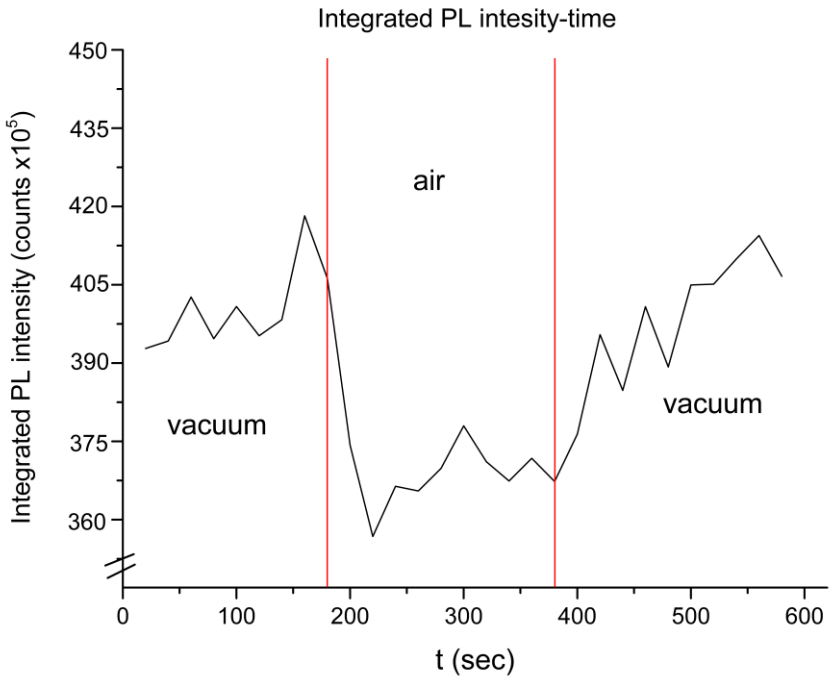

Figure 4.9: Diagram of integrated PL intensities to wavelength related to time on sample of a 3D nest deposited with ZnO nanorods but on flat area. As indicated, it seems that there was sensing behavior since the change of environment induces changes in the PL intensity.

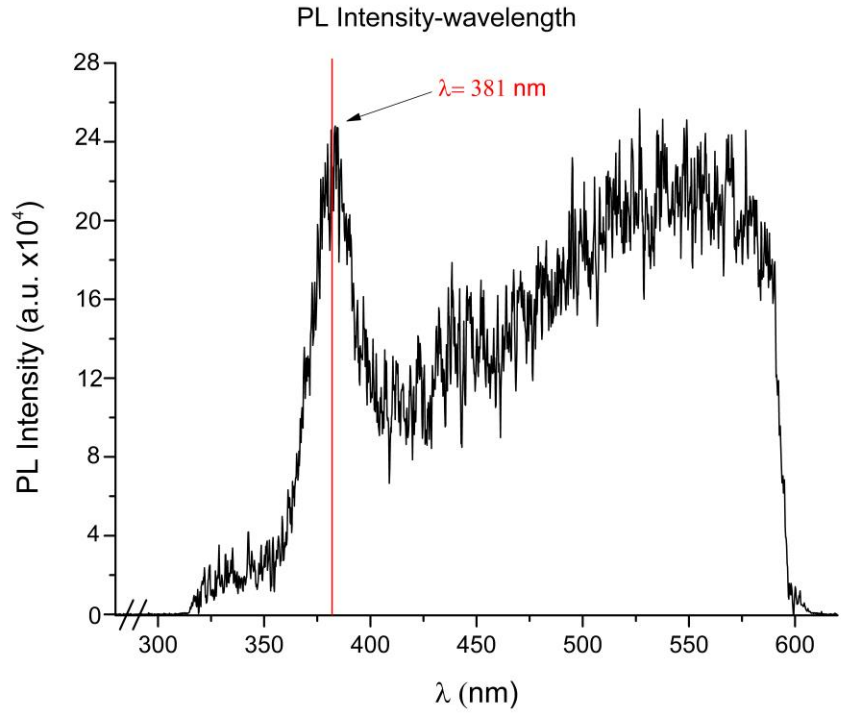

Figure 4.10: Diagram of PL intensity related to wavelength on sample of a 3D nest deposited with ZnO nanorods. PL peek is centered at 381nm as expected due to ZnO bandgap energy. Impurities in crystal lattice are responsible for increase on light wavelength emission.

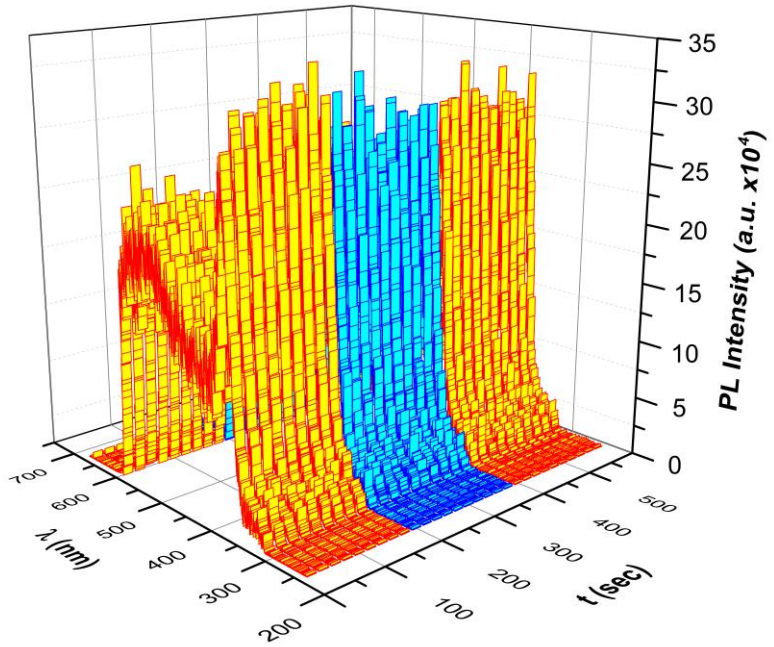

Figure 4.11: Diagram of PL intensities related to wavelength and time on sample of a 3D nest deposited with ZnO nanorods. There was change in the environment of 3D nest, yellow measurements represent vacuum environment and blue measurements represent air environment.

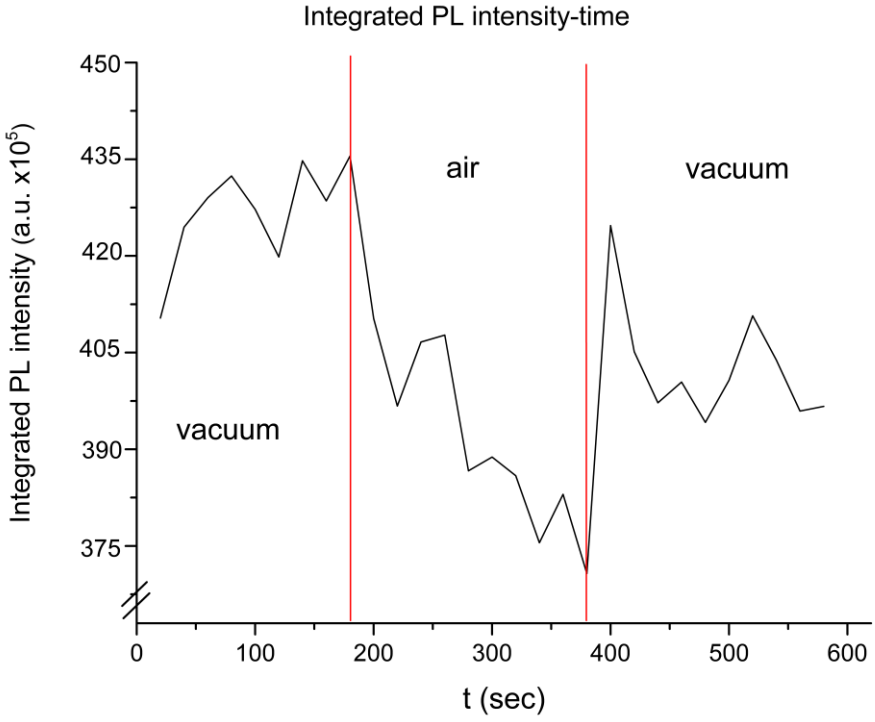

Figure 4.12: Diagram of integrated PL intensities to wavelength related to time on sample of a 3D nest deposited with ZnO nanorods. As indicated, it seems that there was sensing behavior since the change of environment induces changes in the PL intensity.

4.4 Growth of ZnO nanorods on flat substrates related to PLD

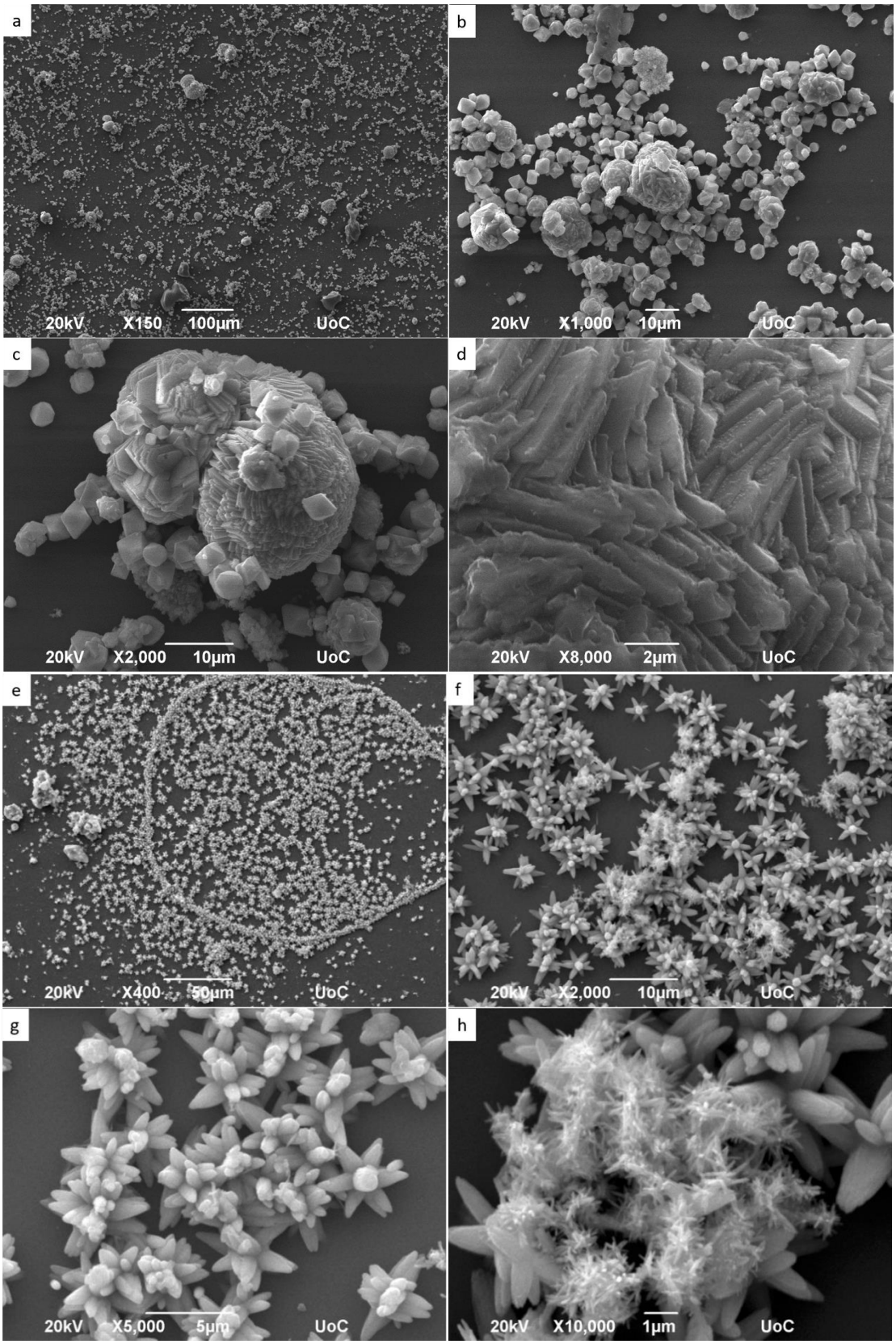

Figure 4.13: SEM images of ZnO nanorods with seed layer of Zn and with growth time 3 hours , a),b),c),d) the result of ACG procedure when the template where pyrex glass bottle with growth solution was localized, was preheated, e),f),g),h) the result of ACG procedure when solution had much higher pH.

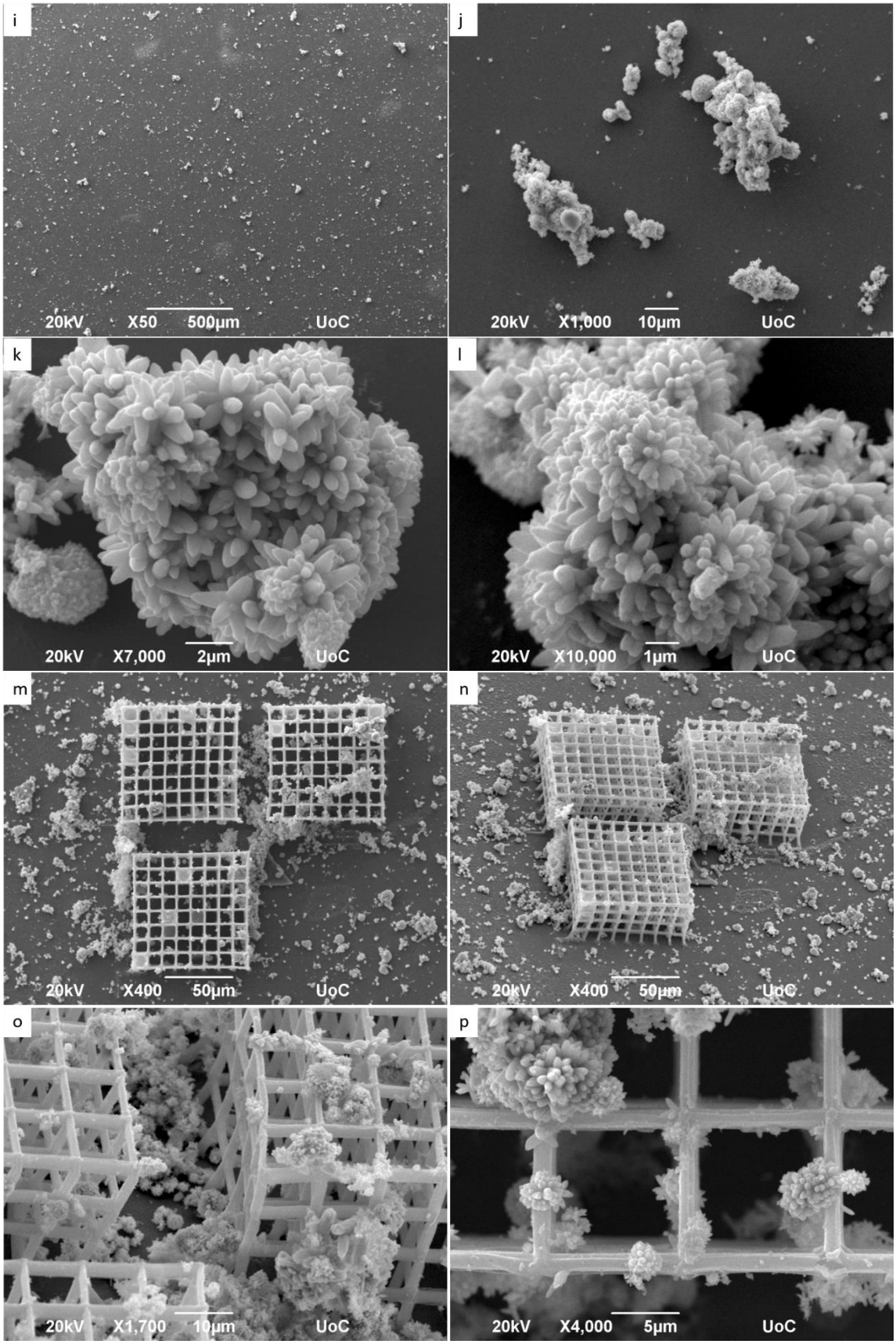

Figure 4.14: SEM images of ZnO nanorods without seed layer of Zn and with growth time 2 hours, i),j),k),l) the result of ACG procedure when solution has higher pH and template was preheated, m),n),o),p) SEM images of 3D grids deposited with ZnO nanorods and without seed layer of Zn at different zoom in images.

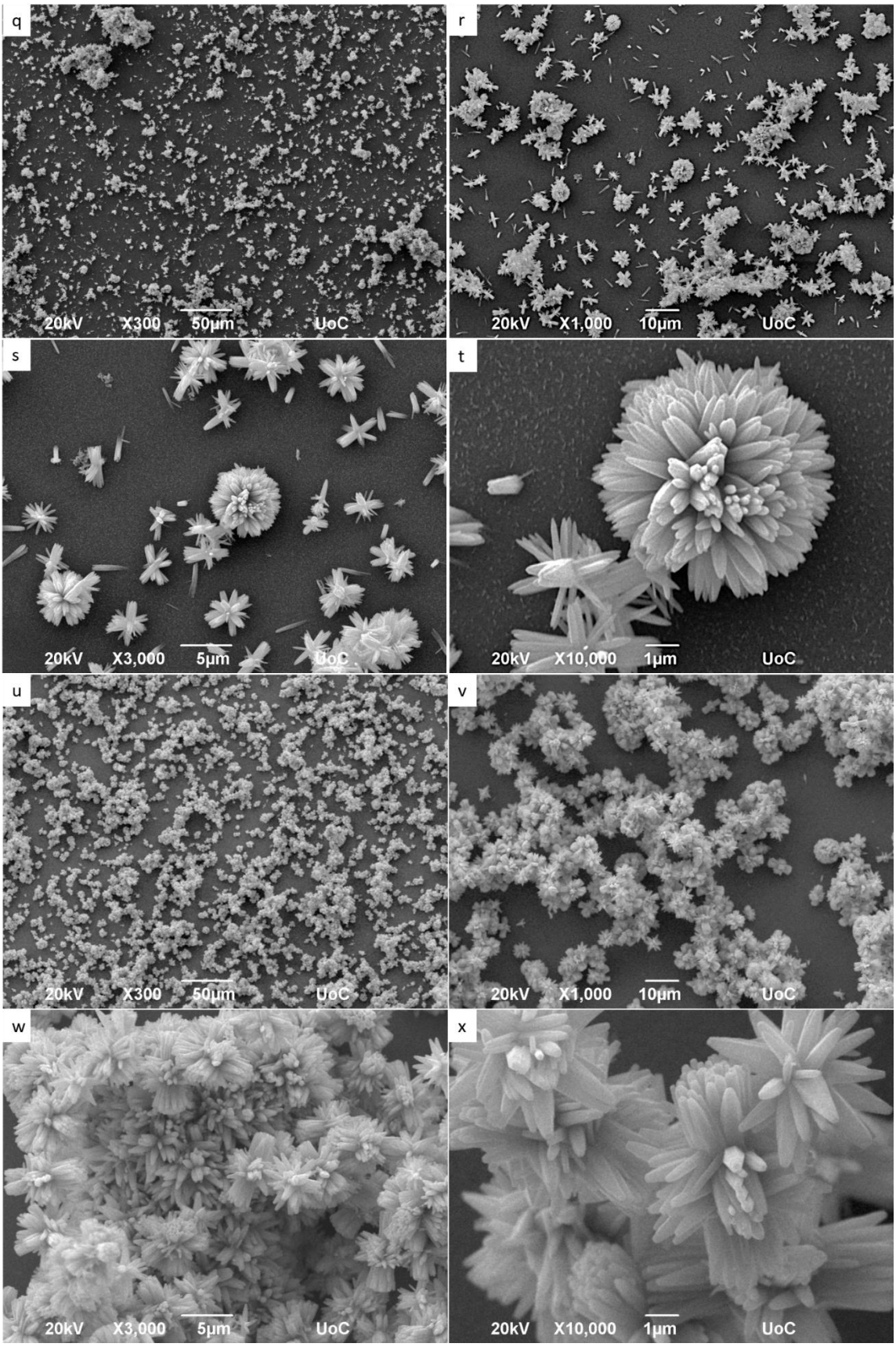

Figure 4.15: SEM images of ZnO nanorods without seed layer of Zn and with growth time 2,5 hours, q),r),s),t)) the result of ACG procedure when solution has little bit higher pH and template was preheated, u),v),w),x) the result of ACG with same parameters but template wasn't preheated.

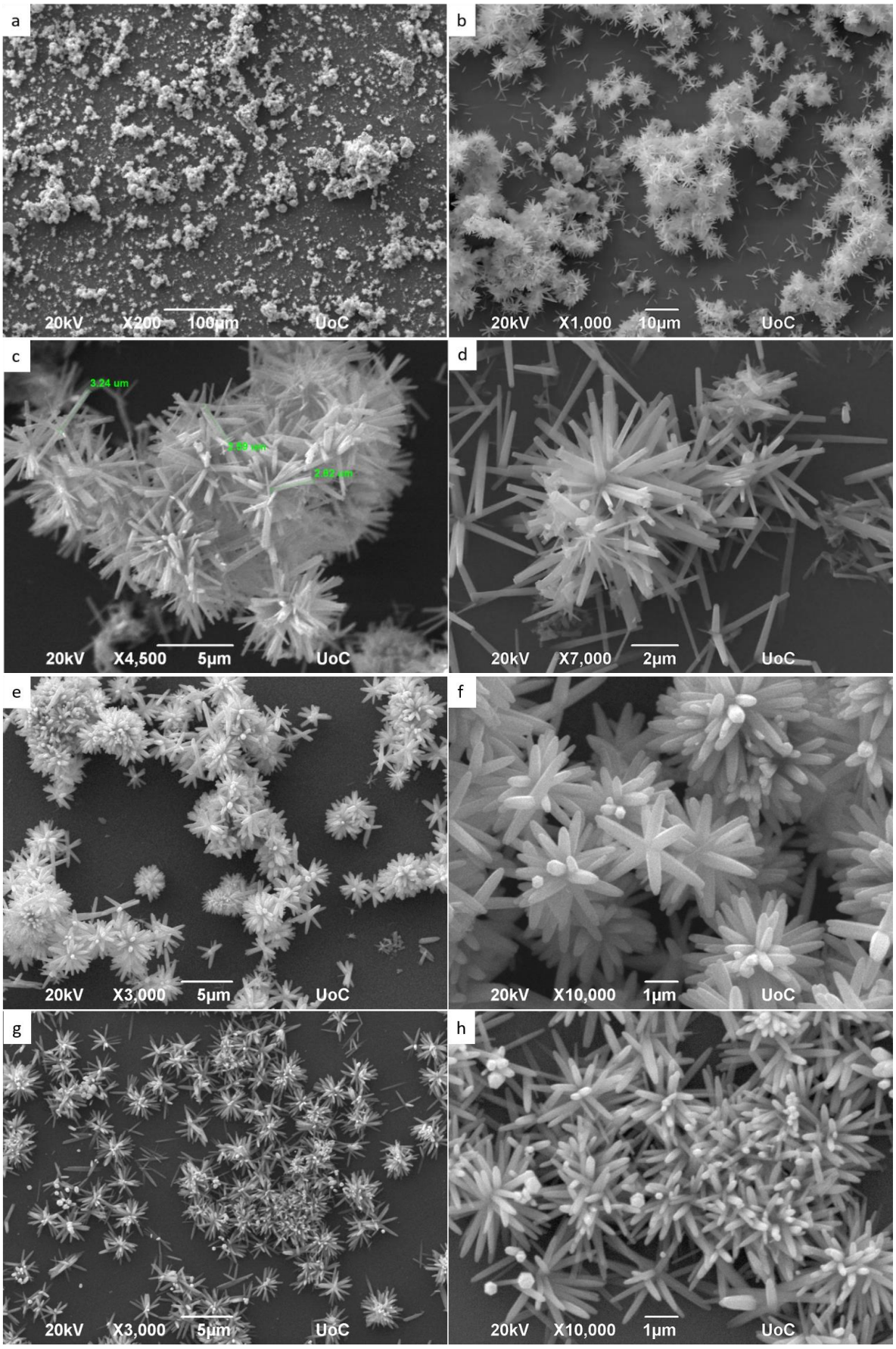

Figure 4.16: SEM images of ZnO nanorods without seed layer of Zn in different zoom in images, a),b),c),d) with growth time 3 hours, e),f),g),h) with growth time 2,5 hours.

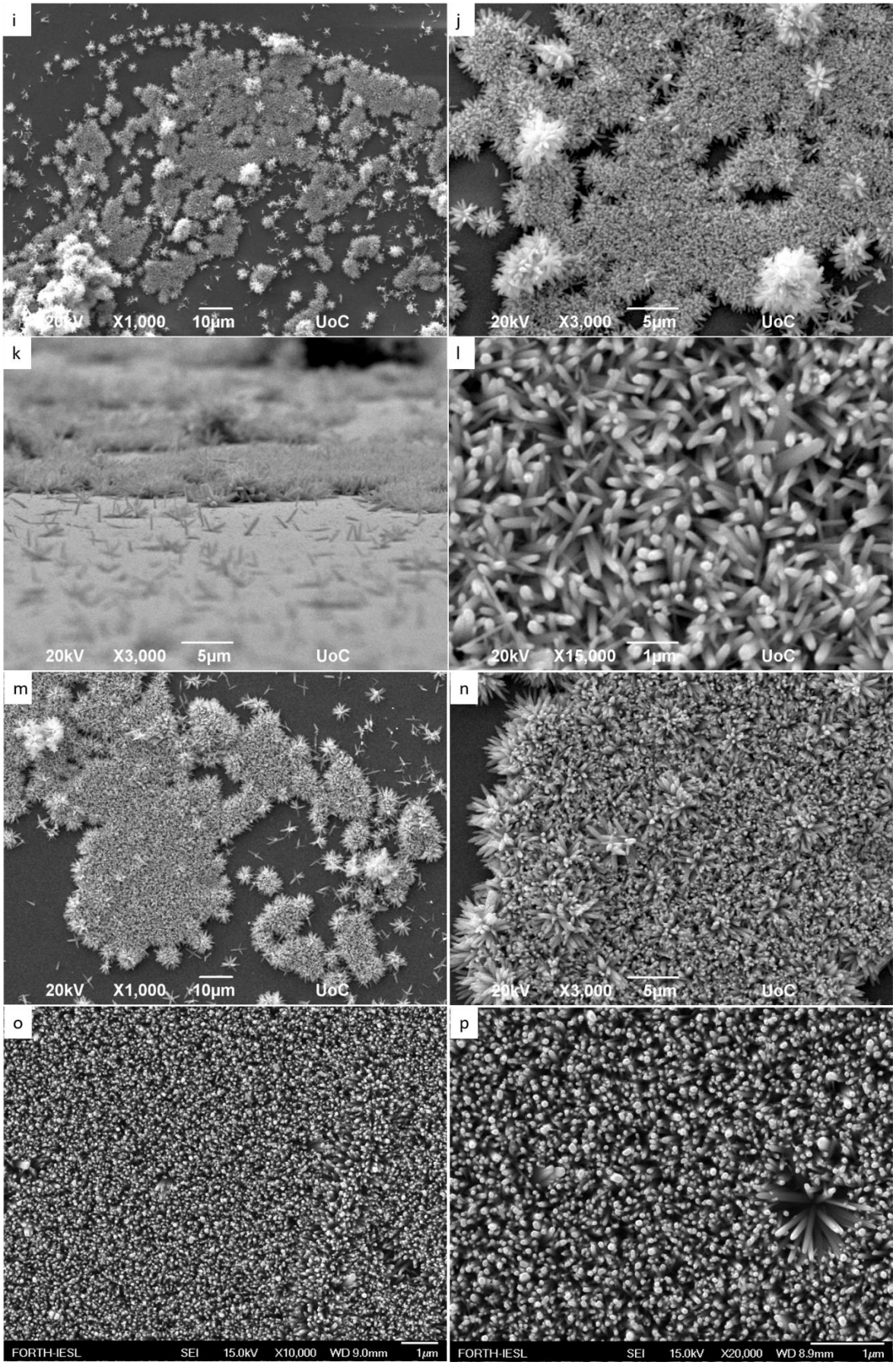

Figure 4.17: i),j),k),l),m),n) SEM images of ZnO nanorods with growth time 2 hours and without seed layer of Zn in different zoom in images, o),p) SEM images of 3D grids deposited with seed layer of Zn at different zoom in images.

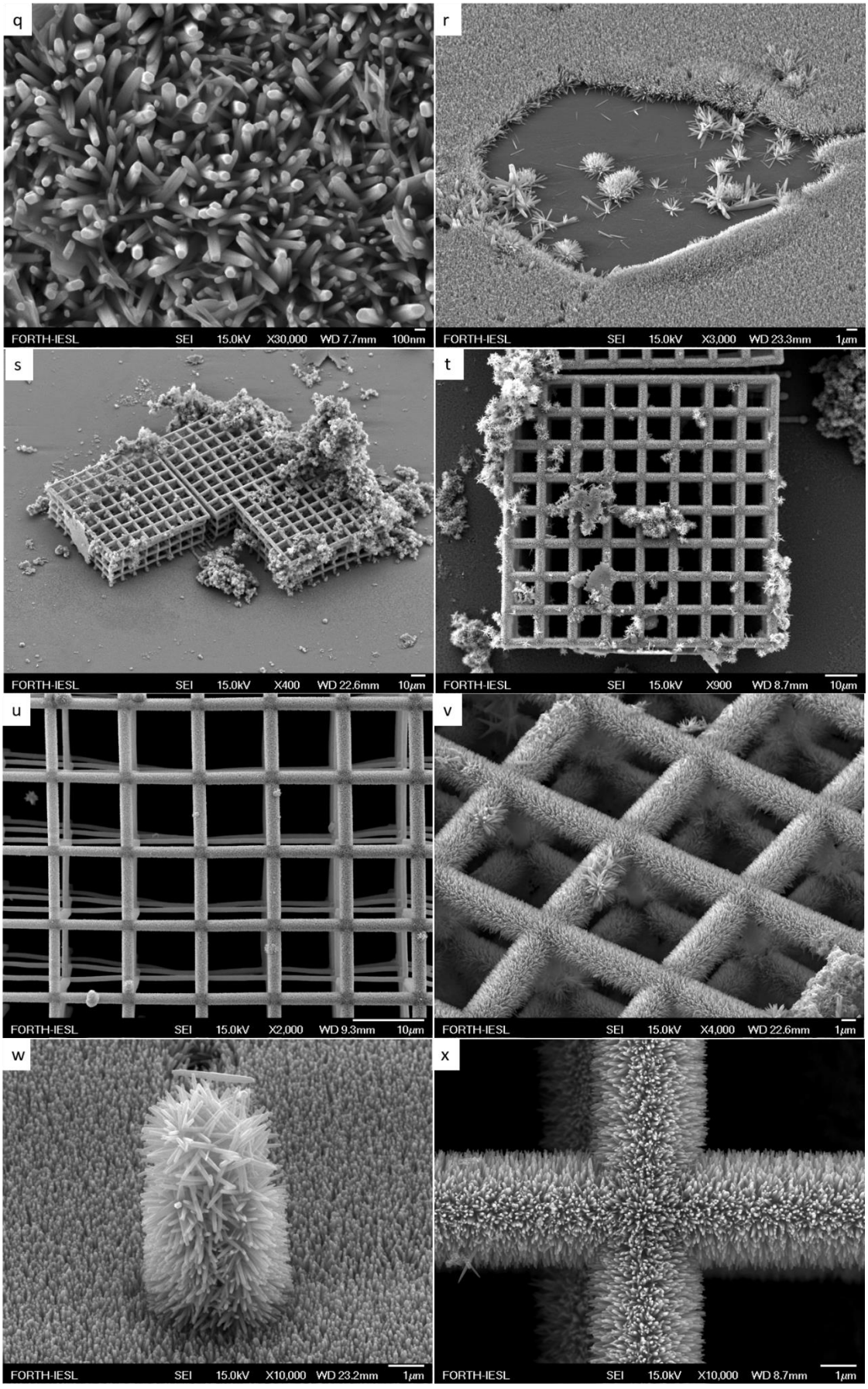

Figure 4.18: SEM images of ZnO nanorods with seed layer of Zn with growth time 2,5 hours, q),r) ZnO nanorods on flat substrate, s),t) without bottom-up localization, u),v) growth time 1,5 hours but uniformly aligned ZnO nanorods, w),x) growth time 2 hours.

Conclusions

3D structures consisted of ZnO nanorods were fabricated using procedures of MPL, PLD and ACG. After investigation, there was confirmed that ZnO nanorod length increases with growth solution. Diagrams of PL intensity were obtained, related to wavelength on sample of a 3D nest deposited with ZnO nanorods. PL peek was centered at 381nm as expected due to ZnO bandgap energy. Impurities in crystal lattice are responsible for reduction on light wavelength emission. PL emissions can be used as sensing parameter. Sensing behavior at room temperature of these samples was investigated and atmospheric air and vacuum were utilized as environments. There is not important difference in sensing behavior on ZnO nanorods, either they were fabricated on flat substrates or 3D structures. As a result, there must be more investigation about increasing of sensing behavior related to increasing of active surface area.

References

1. Sun, H. B. & Kawata, S. Two-photon photopolymerization and 3D lithographic microfabrication. *Adv. Polym. Sci.* **170**, 169–273 (2004).

2. Arnold, C. B. & Piqué, A. L aser Direct-Write Processing. **32**, 9–15 (2018).

3. Jain, K., Rice, S. & Lin, B. J. Ultrafast deep UV lithography using excimer lasers. *Polym. Eng. Sci.* **23**, 1019–1021 (1983).

4. Jonušauskas, L. & Gailevičius, D. Mesoscale Laser 3D Printing. 15205–15221 (2019). doi:10.1364/OE.27.015205

5. Lewis, J. A. & Gratson, G. M. Direct writing in three dimensions. *Mater. Today* **7**, 32–39 (2004).

6. Vieu, C. *et al.* Electron beam lithography : resolution limits and applications. 111–117 (2000).

7. Watt, F. & Bettiol, A. A. ION BEAM LITHOGRAPHY AND NANOFABRICATION : A REVIEW. *Int. J. Nanosci.* **4**, 269–286 (2005).

8. Farsari, M., Vamvakaki, M. & Chichkov, B. N. Multiphoton polymerization of hybrid materials. *J. Opt.* **12**, (2010).

9. Farsari, M. & Selimis, A. High-resolution 3D prototyping. *SPIE Newsroom* 7–9 (2014). doi:10.1117/2.1201410.005651

10. Sakellari, I. *et al.* Quantum dot based 3D printed woodpile photonic crystals tuned for the visible. *Nanoscale Adv.* **1**, 3413–3423 (2019).

11. Sugawara, M., Yamamoto, T. & Ebe, H. Quantum-dot-based photonic devices. *Fujitsu Sci. Tech. J.* **43**, 495–501 (2007).

12. Bickauskaite, G. *et al.* 3D Photonic Nanostructures via Diffusion-Assisted Direct fs Laser Writing. **2012**, (2012).

13. Vasilantonakis, N. *et al.* Three-Dimensional Metallic Photonic Crystals with Optical Bandgaps. 1101–1105 (2012). doi:10.1002/adma.201104778

14. Giakoumaki, A. N. *et al.* 3D micro-structured arrays of ZnO nanorods /639/166 /639/925 /142/126 article. *Sci. Rep.* **7**, 1–9 (2017).

15. Aristov, A. I. *et al.* 3D plasmonic crystal metamaterials for ultra-sensitive biosensing. *Nat. Publ. Gr.* 1–8 (2016). doi:10.1038/srep25380

16. Melissinaki, V., Farsari, M. & Pissadakis, S. A fiber optic Fabry-Perot cavity sensor for the probing of oily samples. *Fibers* **5**, 1–10 (2017).

17. Melissinaki, V., Farsari, M. & Pissadakis, S. A Fiber-endface, fabry-perot vapor microsensor fabricated by multiphoton polymerization. *IEEE J. Sel. Top. Quantum Electron.* **21**, (2015).

18. Giakoumaki, A. N. *et al.* 3D patterning of ZnO nanostructures. *Mater. Today* **20**, 392–393 (2017).

19. Sakellari, I. *et al.* 3D Chiral Plasmonic Metamaterials Fabricated by Direct Laser Writing: The Twisted Omega Particle. *Adv. Opt. Mater.* **5**, 1–6 (2017).

20. Drakakis, T. S. *et al.* Construction of three-dimensional biomolecule structures employing femtosecond lasers Construction of three-dimensional biomolecule structures employing femtosecond lasers. **144108**, 1–4 (2015).

21. Xing, J. F., Zheng, M. L. & Duan, X. M. Two-photon polymerization microfabrication of hydrogels: an advanced 3D printing technology for tissue engineering and drug delivery. *Chem. Soc. Rev.* **44**, 5031–5039 (2015).

22. Psycharakis, S., Tosca, A., Melissinaki, V., Giakoumaki, A. & Ranella, A. Tailor-made three-dimensional hybrid scaffolds for cell cultures. *Biomed. Mater.* **6**, (2011).

23. Melissinaki, V. *et al.* Direct laser writing of 3D scaffolds for neural tissue engineering applications. *Biofabrication* **3**, (2011).

24. Schizas, C. *et al.* On the design and fabrication by two-photon polymerization of a readily assembled micro-valve. *Int. J. Adv. Manuf. Technol.* **48**, 435–441 (2010).

25. Kabouraki, E. *et al.* Redox multiphoton polymerization for 3D nanofabrication. *Nano Lett.* **13**, 3831–3835 (2013).

26. LaFratta, C. N., Fourkas, J. T., Baldacchini, T. & Farrer, R. A. Multiphoton fabrication. *Angew. Chemie - Int. Ed.* **46**, 6238–6258 (2007).

27. Chichkov, B. N. Two-Photon Polymerization: A New Approach to Micromachining. (2006).

28. Farsari, M. & Chichkov, B. N. Materials processing: Two-photon fabrication. *Nat. Photonics* **3**, 450–452 (2009).

29. Malinauskas, M., Farsari, M., Piskarskas, A. & Juodkazis, S. Ultrafast laser nanostructuring of photopolymers: A decade of advances. *Phys. Rep.* **533**, 1–31 (2013).

30. Lee, K. S., Kim, R. H., Yang, D. Y. & Park, S. H. Advances in 3D nano/microfabrication using two-photon initiated polymerization. *Prog. Polym. Sci.* **33**, 631–681 (2008).

31. Lee, K. S., Yang, D. Y., Park, S. H. & Kim, R. H. Recent developments in the use of two-photon polymerization in precise 2D and 3D microfabrications. *Polym. Adv. Technol.* **17**, 72–82 (2006).

32. Obata, K., El-tamer, A., Koch, L., Hinze, U. & Chichkov, B. N. High-aspect 3D two-photon polymerization structuring with widened objective working range (WOW-2PP). 8–11 (2013). doi:10.1038/lsa.2013.72

33. Juodkazis, S. *et al.* Three-dimensional microfabrication of materials by femtosecond lasers for photonics applications APPLIED PHYSICS REVIEWS — FOCUSED REVIEW Three-dimensional microfabrication of materials by femtosecond lasers for photonics applications. **051101**, (2011).

34. Taylor, P., Tan, B., Venkatakrishnan, K. & Makaronets, A. Designed Monomers and Polymers Effects of pulsewidth on two-photon polymerization. 37–41 (2012). doi:10.1080/15685551.2012.705502

35. Sakellari, I. *et al.* Diffusion-assisted high-resolution direct femtosecond laser writing. *ACS Nano* **6**, 2302–2311 (2012).

36. Selimis, A. & Farsari, M. Hybrid Materials for Multiphoton Polymerization. 167–181 (2017).

37. Ovsianikov, A. *et al.* Two-photon polymerization of hybrid sol-gel materials for photonics applications. *Laser Chem.* **2008**, (2008).

38. Kabouraki, E. *et al.* Direct fs Laser Writing of 3D Nanostructures. doi:10.1007/978-3-319-12217-5

39. Ovsianikov, A. *et al.* Ultra-low shrinkage hybrid photosensitive material for two-photon polymerization microfabrication. *ACS Nano* **2**, 2257–2262 (2008).

40. Ovsianikov, A. *et al.* Shrinkage of microstructures produced by two-photon polymerization of Zr-based hybrid photosensitive materials. *Opt. Express* **17**, 2143 (2009).

41. Giakoumaki, I. S. A. G. A., Fotakis, D. G. C., Vamvakaki, M. F. M. & Chichkov, C. R. A. O. B. N. Two-photon polymerization of titanium-containing sol – gel composites for three-dimensional structure fabrication. 359–364 (2010). doi:10.1007/s00339-010-5864-0

42. Farsari, M. 3D Printing via Multiphoton Polymerization. 83–105 (2017).

43. Selimis, A., Mironov, V. & Farsari, M. Microelectronic Engineering Direct laser writing : Principles and materials for scaffold 3D printing. *Microelectron. Eng.* 1–7 (2014). doi:10.1016/j.mee.2014.10.001

44. Boyd, I. W. Thin film growth by pulsed laser deposition. *Laser Ion Beam Modif. Mater.* **8842**, 319–326 (1994).

45. Fujioka, H. *Pulsed Laser Deposition (PLD). Handbook of Crystal Growth: Thin Films and Epitaxy: Second Edition* **3**, (Elsevier B.V., 2014).

46. Norton, D. P. Pulsed laser deposition of complex materials: Progress toward applications. *Pulsed Laser Depos. Thin Film. Appl. Growth Funct. Mater.* 1–31 (2006). doi:10.1002/9780470052129.ch1

47. Schneider, C. W. & Lippert, T. ChemInform Abstract: Laser Ablation and Thin Film Deposition. *ChemInform* **42**, no-no (2011).

48. Carlsson, J. & Martin, P. M. *Chemical Vapor Deposition. Handbook of Deposition Technologies for Films and Coatings* (Elsevier Ltd., 2010). doi:10.1016/B978-0-8155-2031-3.00007-7

49. Liu, Y. *et al.* Ultraviolet Detectors Based on Epitaxial ZnO Films Grown by MOCVD. 69–74 (2000).

50. Beam, M. & Mbe, E. Basics of Molecular Beam Epitaxy (MBE) technique CHAPTER 4. (2016).

51. Dijkkamp, D. *et al.* Preparation of Y-Ba-Cu oxide superconductor thin films using pulsed laser evaporation from high Tc bulk material. *Appl. Phys. Lett.* **51**, 619–621 (1987).

52. Sanz, M. *et al.* Femtosecond laser deposition of TiO 2 by laser induced forward transfer. *Thin Solid Films* **518**, 5525–5529 (2010).

53. Mateus, R. *et al.* Surface & Coatings Technology Helium load on W-O coatings grown by pulsed laser deposition. **355**, 215–221 (2018).

54. Marozau, I. *et al.* One-step preparation of N-doped strontium titanate films by pulsed laser deposition. *Appl. Phys. A Mater. Sci. Process.* **89**, 933–940 (2007).

55. Singh, R. K. & Narayan, J. Pulsed-laser evaporation technique for deposition of thin films: Physics and theoretical model. *Phys. Rev. B* **41**, 8843–8859 (1990).

56. Willmott, P. R. & Huber, J. R. Pulsed laser vaporization and deposition. *Rev. Mod. Phys.* **72**, 315–328 (2000).

57. Svendsen, W., Schou, J., Thestrup, B. & Ellegaard, O. Ablation from metals induced by visible and UV laser irradiation. *Appl. Surf. Sci.* **96**–**98**, 518–521 (1996).

58. Gamaly, E. G., Rode, A. V. & Luther-Davies, B. Ultrafast Laser Ablation and Film Deposition. *Pulsed Laser Depos. Thin Film. Appl. Growth Funct. Mater.* 99–129 (2006). doi:10.1002/9780470052129.ch5

59. Perrière, J. *et al.* Comparison between ZnO films grown by femtosecond and nanosecond laser ablation. *J. Appl. Phys.* **91**, 690–696 (2002).

60. Leitz, K. H., Redlingshöer, B., Reg, Y., Otto, A. & Schmidt, M. Metal ablation with short and ultrashort laser pulses. *Phys. Procedia* **12**, 230–238 (2011).

61. Lahaye, N. L., Harilal, S. S., Diwakar, P. K. & Hassanein, A. The effect of laser pulse duration on ICP-MS signal intensity, elemental fractionation, and detection limits in fs-LA-ICP-MS. *J. Anal. At. Spectrom.* **28**, 1781–1787 (2013).

62. Ristoscu, C. *et al.* Effects of pulse laser duration and ambient nitrogen pressure in PLD of AlN. *Appl. Phys. A Mater. Sci. Process.* **79**, 927–929 (2004).

63. Joshy, N. V, Saji, K. J. & Jayaraj, M. K. Spatial and temporal studies of laser ablated ZnO plasma. **053307**, (2012).

64. Claeyssens, F. *et al.* Studies of the plume accompanying pulsed ultraviolet laser ablation of zinc oxide Studies of the plume accompanying pulsed ultraviolet laser ablation of zinc oxide. **6886**, (2014).

65. Rijnders, G. & Blank, D. H. A. Growth Kinetics During Pulsed Laser Deposition. *Pulsed Laser Depos. Thin Film. Appl. Growth Funct. Mater.* 177–190 (2006). doi:10.1002/9780470052129.ch8

66. Gupta, S. L., Pandey, P. K. & Thareja, R. K. Dynamics of laser ablated colliding plumes. **013511**, 1–10 (2013).

67. Kim, S. Y., Lee, J. H., Kim, J. J. & Heo, Y. W. Effects of temperature, target/substrate distance, and background pressure on growth of ZnO nanorods by pulsed laser deposition. *J. Nanosci. Nanotechnol.* **14**, 9020–9024 (2014).

68. Li, M. *et al.* Pulsed laser deposition of YBCO thin films on IBAD-YSZ substrates. *Supercond. Sci. Technol.* **16**, 105–109 (2003).

69. Claeyssens, F., Klini, A., Mourka, A. & Fotakis, C. Laser patterning of Zn for ZnO nanostructure growth: Comparison between laser induced forward transfer in air and in vacuum. *Thin Solid Films* **515**, 8529–8533 (2007).

70. Hasabeldaim, E. *et al.* Effect of PLD growth atmosphere on the physical properties of ZnO:Zn thin films. *Opt. Mater. (Amst).* **74**, 76–85 (2017).

71. Geohegan, D. B. & Puretzky, A. A. Dynamics of laser ablation plume penetration through low pressure background gases. *Appl. Phys. Lett.* **67**, 197 (1995).

72. Marozau, I. *et al.* RF-plasma assisted pulsed laser deposition of nitrogen-doped SrTiO 3 thin films. *Appl. Phys. A Mater. Sci. Process.* **93**, 721–727 (2008).

73. Ohshima, T. *et al.* Laser-ablated plasma for deposition of ZnO thin films on various substrates. *Sci. Technol. Adv. Mater.* **2**, 517–523 (2001).

74. Shao, J. *et al.* Low-temperature c -axis oriented growth of nanocrystalline ZnO thin films on Si substrates by plasma assisted pulsed laser deposition. *J. Vac. Sci. Technol. B Microelectron. Nanom. Struct.* **26**, 214–218 (2008).

75. Spanos, I., Selimis, A. & Farsari, M. 3D magnetic microstructures. *Procedia CIRP* **74**, 349–352 (2018).

76. Konstantaki, M., Klini, A., Anglos, D. & Pissadakis, S. An ethanol vapor detection probe based on a ZnO nanorod coated optical fiber long period grating. *Opt. Express* **20**, 8472 (2012).

77. Klini, A., Manousaki, A., Anglos, D. & Fotakis, C. Growth of ZnO thin films by ultraviolet pulsed-laser ablation: Study of plume dynamics. *J. Appl. Phys.* **98**, (2005).

78. Özgür, H. M. and Ü. *Zinc Oxide: Fundamentals, Materials and Device Technology*.

79. Rodnyi, P. A. & Khodyuk, I. V. Optical and luminescence properties of zinc oxide (Review). *Opt. Spectrosc. (English Transl. Opt. i Spektrosk.* **111**, 776–785 (2011).

80. Klini, A. *et al.* ZnO-PDMS nanohybrids: A novel optical sensing platform for ethanol vapor detection at room temperature. *J. Phys. Chem. C* **119**, 623–631 (2015).

81. Wang, L. *et al.* ZnO nanorod gas sensor for ethanol detection. *Sensors Actuators, B Chem.* **162**, 237–243 (2012).

82. Xu, J., Han, J., Zhang, Y., Sun, Y. & Xie, B. Studies on alcohol sensing mechanism of ZnO based gas sensors. *Sensors Actuators, B Chem.* **132**, 334–339 (2008).

83. Kenanakis, G., Vernardou, D., Koudoumas, E., Kiriakidis, G. & Katsarakis, N. Ozone sensing properties of ZnO nanostructures grown by the aqueous chemical growth technique. *Sensors Actuators, B Chem.* **124**, 187–191 (2007).

84. Sanchez-Valencia, J. R. *et al.* Oxygen optical sensing in gas and liquids with nanostructured ZnO thin films based on exciton emission detection. *J. Phys. Chem. C* **118**, 9852–9859 (2014).

85. Zhang, Y. *et al.* Scanning probe study on the piezotronic effect in ZnO nanomaterials and nanodevices. *Adv. Mater.* **24**, 4647–4655 (2012).

86. AlZoubi, T., Qutaish, H., Al-Shawwa, E. & Hamzawy, S. Enhanced UV-light detection based on ZnO nanowires/graphene oxide hybrid using cost-effective low temperature hydrothermal process. *Opt. Mater. (Amst).* **77**, 226–232 (2018).

87. Eom, T. H. & Han, J. I. Single fiber UV detector based on hydrothermally synthesized ZnO nanorods for wearable computing devices. *Appl. Surf. Sci.* **428**, 233–241 (2018).

88. Zhang, J., Tan, T., Zhao, Y. & Liu, N. Preparation of ZnO nanorods/graphene composite anodes for high-performance lithium-ion batteries. *Nanomaterials* **8**, (2018).

89. Zhang, M. L. *et al.* High efficiency solar cell based on ZnO nanowire array prepared by different growth methods. *RSC Adv.* **4**, 10462–10466 (2014).

90. Saboor, A., Shah, S. M. & Hussain, H. Band gap tuning and applications of ZnO nanorods in hybrid solar cell: Ag-doped verses Nd-doped ZnO nanorods. *Mater. Sci. Semicond. Process.* **93**, 215–225 (2019).

91. Sh. Atabaev, T. Size-dependent water splitting activity of ZnO nanorods. *Mater. Today Proc.* **6**, 15–18 (2019).

92. Wang, T., Lv, R., Zhang, P., Li, C. & Gong, J. Au nanoparticle sensitized ZnO nanopencil arrays for photoelectrochemical water splitting. *Nanoscale* **7**, 77–81 (2015).

93. Sun, Y., Fuge, G. M. & Ashfold, M. N. R. Growth of aligned ZnO nanorod arrays by catalyst-free pulsed laser deposition methods. *Chem. Phys. Lett.* **396**, 21–26 (2004).

94. Dash, P., Manna, A., Mishra, N. C. & Varma, S. Synthesis and characterization of aligned ZnO nanorods for visible light photocatalysis. *Phys. E Low-Dimensional Syst. Nanostructures* **107**, 38–46 (2019).

95. Viter, R. *et al.* Photoluminescence immunosensor based on bovine leukemia virus proteins immobilized on the ZnO nanorods. *Sensors Actuators, B Chem.* **285**, 601–606 (2019).

96. Viter, R. *et al.* Bioanalytical system for detection of cancer cells with photoluminescent ZnO nanorods. *Nanotechnology* **27**, 1–11 (2016).

97. Tamashevski, A. *et al.* Zinc oxide nanorod based immunosensing platform for the determination of human leukemic cells. *Talanta* **200**, 378–386 (2019).

98. Zhao, J. H., Liu, C. J. & Lv, Z. H. Photoluminescence of ZnO nanoparticles and nanorods. *Optik (Stuttg).* **127**, 1421–1423 (2016).

99. Kenanakis, G., Androulidaki, M., Vernardou, D., Katsarakis, N. & Koudoumas, E. Photoluminescence study of ZnO structures grown by aqueous chemical growth. *Thin Solid Films* **520**, 1353–1357 (2011).

100. Wei, Y. *et al.* Hydrothermal synthesis of Ag modified ZnO nanorods and their enhanced ethanol-sensing properties. *Mater. Sci. Semicond. Process.* **75**, 327–333 (2018).

101. Naz, H., Ali, R. N., Liu, Q., Yang, S. & Xiang, B. Niobium doped zinc oxide nanorods as an electron transport layer for high-performance inverted polymer solar cells. *J. Colloid Interface Sci.* **512**, 548–554 (2018).

102. Yang, X. *et al.* Nitrogen-doped ZnO nanowire arrays for photoelectrochemical water splitting. *Nano Lett.* **9**, 2331–2336 (2009).

103. Sun, X. W., Yang, Y. & Applications, T. *Nanostructures ZnO ZnO ZnO Nanostructure ZnO Nanostructures*.

104. Klini, A., Mourka, A., Dinca, V., Fotakis, C. & Claeyssens, F. ZnO nanorod micropatterning via laser-induced forward transfer. *Appl. Phys. A Mater. Sci. Process.* **87**, 17–22 (2007).

105. Bhushan, B., Murty, B. S. & Mondal, K. A new approach for synthesis of ZnO nanorod flowerets and subsequent pure free-standing ZnO nanorods. *Adv. Powder Technol.* **30**, 30–41 (2019).

106. Vayssieres, L., Guo, J. & Nordgren, J. Aqueous Chemical Growth of α-Fe 2O 3-α-Cr 2O 3 Nanocomposite Thin Films. *J. Nanosci. Nanotechnol.* **1**, 385–388 (2001).

107. Kenanakis, G. & Katsarakis, N. Chemically grown TiO2 on glass with superior photocatalytic properties. *J. Environ. Chem. Eng.* **2**, 1748–1755 (2014).

108. Morko, H. & zgr, mit. ZnO Nanostructures. *Zinc Oxide* 365–386 (2009). doi:10.1002/9783527623945.ch7

109. Greene, L. E. *et al.* Low-temperature wafer-scale production of ZnO nanowire arrays. *Angew. Chemie - Int. Ed.* **42**, 3031–3034 (2003).

110. Benavente Llorente, V., Vázquez, C. I., Burgos, M. A., Baruzzi, A. M. & Iglesias, R. A. Charge transport on vertically aligned ZnO nanorods with different aspect ratios. *Electrochim. Acta* **319**, 990–997 (2019).

111. Vernardou, D. *et al.* pH effect on the morphology of ZnO nanostructures grown with aqueous chemical growth. *Thin Solid Films* **515**, 8764–8767 (2007).

112. Rayerfrancis, A., Balaji Bhargav, P., Ahmed, N., Chandra, B. & Dhara, S. Effect of pH on the morphology of ZnO nanostructures and its influence on structural and optical properties. *Phys. B Condens. Matter* **457**, 96–102 (2015).

113. Singh, O., Singh, M. P., Kohli, N. & Singh, R. C. Effect of pH on the morphology and gas sensing properties of ZnO nanostructures. *Sensors Actuators, B Chem.* **166**–**167**, 438–443 (2012).

114. Vernardou, D. *et al.* The effect of growth time on the morphology of ZnO structures deposited on Si (1 0 0) by the aqueous chemical growth technique. *J. Cryst. Growth* **308**, 105–109 (2007).

115. Gan, A. *et al.* Growth of Uniformly Aligned ZnO Nanowire Heterojunction. 7920–7923 (2005).

116. Park, W. Il & Yi, G. C. Electroluminescence in n-ZnO Nanorod Arrays Vertically Grown on p-GaN. *Adv. Mater.* **16**, 87–90 (2004).

117. Alarabi, A. *et al.* Influence of different substrates on ZnO nanorod arrays properties. *Solid State Sci.* **85**, 21–25 (2018).

118. Tak, Y. & Yong, K. Controlled growth of well-aligned ZnO nanorod array using a novel solution method. *J. Phys. Chem. B* **109**, 19263–19269 (2005).

119. Li, Q. *et al.* Fabrication of ZnO nanorods and nanotubes in aqueous solutions. *Chem. Mater.* **17**, 1001–1006 (2005).